molecular pharmaceutics

Article

Cite This: Mol. Pharmaceutics 2019, 16, 1678−1693

pubs.acs.org/molecularpharmaceutics

Novel Oligo-Guanidyl-PEG Carrier Forming Rod-Shaped Polyplexes

Alessio Malfanti,[†] Francesca Mastrotto,[†] Yanxiao Han,[‡] Petr Král,[‡,§] Anna Balasso,[†] Anna Scomparin,[⊥,¶] Sabina Pozzi,[⊥] Ronit Satchi-Fainaro,[⊥] Stefano Salmaso,[†] and Paolo Caliceti*[,†]

[†]Department of Pharmaceutical and Pharmacological Sciences, University of Padova, Via F. Marzolo 5 35131 Padova, Italy

[‡]Department of Chemistry and Department of Physics, University of Illinois at Chicago, Chicago, Illinois 60607, United States

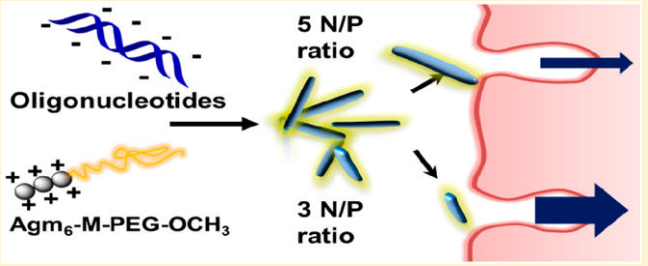
[§]Department of Biopharmaceutical Sciences, University of Illinois at Chicago, Chicago, Illinois 60612, United States

[⊥]Department of Physiology and Pharmacology, Sackler School of Medicine, Tel Aviv University 69978 Tel Aviv, Israel

[¶]Department of Drug Science and Technology, University of Turin, Via P. Giuria 9, 10125 Turin, Italy

Supporting Information

ABSTRACT: A novel unconventional supramolecular oligocationic structure (Agm_6-M-PEG-OCH_3) has been synthesized to yield high efficiency therapeutic oligonucleotide (ON) delivery. Agm_6-M-PEG-OCH_3 was obtained by a multistep protocol that included the conjugation of agmatine (Agm) moieties to maltotriose (M), which was further derivatized with one poly(ethylene glycol) (PEG) chain. Gel electrophoresis analysis showed that the 19 base pairs dsDNA model ON completely associates with Agm_6-M-PEG-OCH_3 at 3 N/P molar ratio, which is in agreement with the *in silico* molecular predictions. Isothermal titration calorimetry (ITC) analyses showed that the Agm_6-M-PEG-OCH_3/ON association occurs through a combination of mechanisms depending on the N/P ratios resulting in different nanostructures. Dynamic light scattering (DLS) and transmission electron microscopy (TEM) revealed that the Agm_6-M-PEG-OCH_3/ON polyplexes have rod-shape structure with a mean diameter of 50−75 nm and aspect ratio depending on the N/P ratio. The polyplexes were stable over time in buffer, while a slight size increase was observed in the presence of serum proteins. Cell culture studies showed that neither Agm_6-M-PEG-OCH_3 nor polyplexes displayed cytotoxic effects. Cellular uptake depended on the cell line and polyplex composition: cellular internalization was higher in the case of MCF-7 and KB cells compared to MC3T3-E1 cells and polyplexes with smaller aspect ratio were taken-up by cells more efficiently than polyplexes with higher aspect ratio. Finally, preliminary studies showed that our novel carrier efficiently delivered ONs into cells providing gene silencing.



KEYWORDS: *oligonucleotides delivery, cationic carriers, polyplexes, nanoparticles, nonviral carriers*

INTRODUCTION

Therapeutic oligonucleotides (ONs, e.g. siRNA, miRNA, etc.) are being exploited in gene therapy to attenuate or override the influence of malfunctioning genes by gene degradation, translational target repression, or silencing.[1−3] Unfortunately, despite the unique opportunities offered by ONs for the treatment of a variety of disorders, they often fail to meet their therapeutic goal because of their degradation by serum nucleases, negligible transmembrane transport, off-target profile, and immunogenic response.[4] Therefore, therapeutic ON discovery has paralleled with the development of viral or nonviral ON delivery carriers that circumvent these limitations.

The use of viral vectors is limited by intrinsic toxicity and immunogenicity, low ON packaging, and difficult scale-up production.[5−8] Nonviral vectors, namely cationic vesicles, nanoparticles, and macromolecules, offer many advantages over viral carriers including biosafety, easy scale-up production, low host immunogenicity, and controlled delivery.

Cationic supramolecular nanocarriers can be generated with a variety of materials such as cationic polymers, knotted structures, dendrimers, cyclodextrins, lipids, and bola-lipids. These macromolecules form polyplexes by electrostatic association with ONs, which protect them from degradation and favor their internalization by endocytic pathways into the diseased cells.[9−11] Nevertheless, most of these cationic macromolecules raise cytotoxic effects as consequence of interactions with cell membranes[12] and present nonspecific interactions with blood components. Furthermore, these nonviral vectors often have low bioavailability and transfection efficiency compared to viral vectors resulting in limited biological outcome.[13−15]

Cationic lipids display different transfection behavior according to their architecture and geometric features; for example, "cone" shaped lipids possess enhanced transfection properties.[16,17] Linear polyethylenimine (PEI), the gold

Received: January 6, 2019
Revised: March 11, 2019
Accepted: March 12, 2019
Published: March 12, 2019

Downloaded via UNIV OF ILLINOIS CHICAGO on May 3, 2019 at 02:11:52 (UTC).
See https://pubs.acs.org/sharingguidelines for options on how to legitimately share published articles.

© 2019 American Chemical Society

DOI: 10.1021/acs.molpharmaceut.9b00014
Mol. Pharmaceutics 2019, 16, 1678−1693

standard polymer for ON and gene delivery, was found to be more efficient in gene transfer compared to the branched polymer, while linear poly [(2-dimethylamino) ethyl methacrylate)] (pDMAEMA) was less effective compared to both hyperbranched and star-like pDMAEMA.[18,19] Cyclic pDMAEMA was shown to possess longer residence time in blood circulation and lower toxicity compared to its linear counterpart, while the transfection efficiency has been found to be markedly influenced by the molecular weight.

The introduction of stealth polymers, namely PEG, into the polycationic macromolecules yields polyplexes that can escape the immunosystem and other clearance processes thus prolonging the residence time in the bloodstream.[20] Furthermore, PEGylation reduces the carrier-induced hemolysis, protects ONs from enzymatic degradation, enhances the colloidal stability, and can target tumor tissues dependent on increased extravasation by the enhanced permeability and retention (EPR) effect.[21] PEG−PEI and PEG-poly-L-Lys polyplexes, for example, have been designed to display extravasation-dependent accumulation in solid tumors where, by virtue of the positive charge, they can be taken-up by the cells.[22,23]

According to the evidence that diblock copolymer and cyclic polymers containing 6−8 cationic groups efficiently form polyplexes[24] that display prolonged residence time in the bloodstream and accumulate in solid tumors, we investigated a novel cationic supramolecular platform where a polycationic "star-like head" formed by six guanidyl units attached to an oligosaccharide core was combined with a PEG "tail". The nonpolymeric and nonpeptidic cationic "star-like head" can provide for Coulombic ON association, while PEG endows polyplexes with biophysical stability.

Here, we report the design, synthesis and characterization of the novel ON carrier formed by a nonlinear oligo-cationic (oligo-guanidyl) "star-like head" and a flexible polymer (PEG) "tail". We observed that this chemical structure can form polyplexes with a peculiar rod shape, which can have relevant impact on their biopharmaceutical behavior. The cell up-take of polyplexes was tested on three model cell lines. Finally, the bioactivity of the new nanoplatform was preliminarily evaluated on human cervical carcinoma HeLa cells. For its role in cell invasion and metastasis, Rac1 gene pathway was selected as a model to evaluate the ability of the novel oligo-cationic polymer (Agm_6-M-PEG-OCH_3) to silence a specific gene.

EXPERIMENTAL SECTION

Materials. Maltotriose, 6-aminocaproic acid, acetic anhydride, 2-bromoisobutyryl bromide, trimethylamine, ascorbic acid, agmatine sulfate, 1-ethyl-3-[3-(dimethylamino)propyl] carbodiimide hydrochloride (EDC), *N*,*N*′-dicyclohexylcarbodiimide (DCC), *N*-hydroxysuccinimide (NHS), xylen cyanol, acryloyl chloride, copper bromide, tris(2-pyridylmethyl)amine (TPMA), deuterated solvents (D_2O, $CDCl_3$), glycerol, tris-(hydroxymethyl)aminomethane chloride (Tris), boric acid, ethylenediaminetetraacetic acid, and thiazole orange were purchased from Sigma-Aldrich (St. Louis, MO, USA). Linear 5 kDa α-methoxy-ω-amino-polyethylene glycol (NH_2−$PEG_{5\ kDa}$-OCH_3) was obtained from Iris Biotech GmbH (Marktredwitz, Germany). Double-strand DNA (dsDNA) and cyanin-3 labeled ds-DNA (Cy3-dsDNA; 19 nucleotides per strand) were purchased from Biomers.net GmbH (Ulm, Germany). The GelRed (dsDNA intercalating agent) was purchased from SICHIM (Rome, Italy). siRNA (Rac1 siRNA, Luciferase siRNA) sequences were from QBI Enterprise (Ness Ziona, Israel). Lipofectamine 2000 was obtained from Life Technologies (Grand Island, NY, USA). The psiCHECK reporter assay was purchased from Promega Cat#E1960 (Madison, Wisconsin, USA). Solvents were furnished by Carlo Erba (Milan, Italy), VWR International (Lutherworth, UK), and Sigma-Aldrich (St. Louis, MO, USA). All the other reagents or salts were obtained from Fluka Analitical or Sigma-Aldrich. Chamber slides BD Falcon for confocal microscopy were purchased from Corning (Tewksbury, MA, USA). Vectashield mounting medium with 4,6-diamidine-2-phenylindole (DAPI) was provided by Vector Laboratories Inc. (Burlingame, CA, U.S.A.).

GPC analyses were performed by using a Malvern Viscotek triple detector array (TDA) model 302, equipped with refractometer, light scattering (low-angle light scattering-LALS and right-angle light scattering-RALS) and differential viscosimeter, and TSKgel G3000 (7 μm, 7.8 × 300 mm^2) and TSKgel G4000 (10 μm, 7.8 × 300 mm^2) Tosoh columns. A set of narrow dispersity polyethylene glycol (PEG) standards (282−30 000 Da, EasiVial PEG Agilent Technologies, Inc.) were used to calibrate the columns. Cell lines from human cervical carcinoma (KB), human breast cancer (MCF-7), murine preosteoblast (MC3T3-E1), and human cervical carcinoma (HeLa) were provided by the cell bank ATCC (Manassas, VA, USA). All products for cell biology including Dulbecco's modified Eagle medium (DMEM), L-glutamine, trypsin, antibiotic and antimicotic solution, fetal bovine serum (FBS), and phosphate saline buffer with and without Ca^{2+}/Mg^{2+},3-(4,5-dimethylthiazol-2-yl)-2,5-diphenyltetrazolium bromide (MTT) were obtained from Sigma-Aldrich (St. Louis, MO, USA).

*Synthesis of Maltotriosyl-N-acetyl-amino-hexanoic Acid (M-COOH) (**1**).* Thirty milliliters of a 34.7 mg/mL 6-aminohexanoic acid solution (0.264 M) in methanol acidified with 1% v/v acetic acid was added of 1 g (1.98 mmol) of maltotriose and heated to 60 °C until complete maltotriose dissolution. The solution was maintained under stirring for 14 h at 50 °C and, after reduction to half volume under vacuum, 22.6 mL of acetic anhydride (237.6 mmol) was added over 60 min and then maintained under stirring at room temperature. After 24 h, the volume was reduced to about 5 mL and dropwise added to 100 mL of cold diethyl ether to precipitate the maltotriosyl-N-acetyl-amino-hexanoic acid (M-COOH). The precipitate was recovered by 5 min centrifugation at 4000 rpm and then desiccated under reduced pressure. The final product, 1.1 g, was analyzed by ^{1}H NMR, ESI-TOF mass spectrometry, FT-IR, and elemental analysis.

^{1}H NMR (400 MHz, D_2O) δ (ppm): 5.34 (s, 1 H, anomeric proton), 5.13 (s, 1 H, anomeric proton), 4.06−3.29 (m, 20 H, sugar region + ε-CH_2), 2.27−2.28 (m, 2 H, α-CH_2), 2.06 (s, 3 H, CH_3−CO−), 1.55 (m, 4 H δ- CH_2 and β-CH_2), 1.24 (m, 2 H, γ-CH_2).

ESI-TOF [m/z]: 658.26 $(M\text{-}H^+)^{1-}$ [calcd. for maltotriosyl-N-acetyl-amino-hexanoic acid 659.26].

FT-IR (KBr): ν (cm^{-1}) 3368 (−OH), 2936 (−CH), 1718 (−COOH), 1623 (acetyl CO-N).

Elemental analysis: C, 44.92%; H, 6.92%; N, 2.78%; (O, 45.38%) [calcd. for maltotriosyl-N-acetyl-amino-hexanoic acid ($C_{26}H_{45}NO_{18}$), C, 47.34%; H, 6.88%; N, 2.12%; O, 43.66%].

*Synthesis of (2-Bromoisobutyryl)$_6$-maltotriosyl-N-acetyl-amino-hexanoic Acid [(isoC$_4$Br)$_6$-M-COOH] (**2**).* The synthesis

DOI: 10.1021/acs.molpharmaceut.9b00014
Mol. Pharmaceutics 2019, 16, 1678−1693

of (2-bromoisobutyryl)$_6$-malytotryosyl-N-acetyl-amino-hexanoic acid [(isoC$_4$Br)$_6$-M-COOH] was performed according to the modified protocol described by Stenzel-Rosembaum et al.[25] A suspension of 1.0 g (1.52 mmol) of maltotriosyl-N-acetyl-amino-hexanoic acid in 40 mL of anhydrous chloroform was added of 4.21 mL (30.2 mmol) of trimethylamine and maintained at 0 °C under stirring for 15 min. Then 3.48 mL (30.2 mmol) of 2-bromo-isobutyryl-bromide was added dropwise over 30 min. The reaction mixture was maintained under stirring for 3 h at 0 °C and then for 72 h at room temperature. The (2-bromoisobutyryl)$_6$-maltotriosyl-N-acetyl-amino-hexanoic acid [(isoC$_4$Br)$_6$-M-COOH] was purified by mixing the reaction mixture with 100 mL of Milli-Q water into a separating funnel. The mixture was then washed three times with 300 mL of cold water, three times with 300 mL of 0.1 N NaOH, and finally three times with 300 mL of cold water. The organic layer containing [(isoC$_4$Br)$_6$-M-COOH] was recovered and dried with anhydrous Na_2SO_4. The suspension was filtered, and the solvent was removed under reduced pressure. The final product, 1.7 g of red−brown oil, was analyzed by ^{1}H NMR, FT-IR and elemental analysis.

^{1}H NMR (400 MHz, $CDCl_3$) δ (ppm): 5.58 (s, 1 H, anomeric proton), 5.25 (s, 1 H, anomeric proton), 4.70−2.53 (m, 20 H, glycosyl scaffold and ε-CH_2), 2.15−1.74 [m, 36 H, CO-$(CH_3)_2$], 1.60 (s, 3 H,-CO−CH_3 acetyl moiety), 1.45−1.06 (m, 4 H, δ- CH_2 and β-CH_2), 1.01−0.67 (m, 2 H, α-CH_2).

FT-IR: 3472 (−OH), 2978 (−CH), 1744 (isobutyryl −CO-O), 1650 (acetyl −CO-N).

Elemental analysis: found C, 40.02%; H, 4.89%; Br, 31.12%; N, 0.84%; (O, 23,13%) [calcd. for (2-bromoisobutyryl)$_6$-maltotryosyl-N-acetyl-amino-hexanoic acid ($C_{50}H_{78}Br_6NO_{24}$), C, 38.66%; H, 4.87%; Br, 30.86%; N, 0.90%; O, 24.72%].

*Synthesis of Acryloyl-agmatine (Acry-Agm) (**3**).* Acryloyl-agmatine (Acry-Agm) was synthesized according to the modified protocol reported in the literature.[26] Briefly, 2.0 g (8.76 mmol) of agmatine sulfate was dissolved at 0 °C in 15 mL of $NaHCO_3$ saturated water solution. The solution was added of 0.75 mL (9.64 mmol) of acryloyl chloride in 30 min under vigorous stirring. After 1 h, the solution pH was adjusted to 1.0 with 1.0 N HCl and the mixture was saturated with sodium chloride. After filtration, acryloyl-agmatine (Acry-Agm) was purified by washing the reaction solution in a separating funnel using 150 mL of ethyl acetate and finally mixed three times with 50 mL of a 1:1 of isopropanol/ethyl acetate solution. The organic fractions were collected, pooled, and concentrated under reduced pressure. A pale-yellow oil was recovered, dissolved in water, and freeze-dried. The final product, 1.0 g, 62% molar yield, was analyzed by ^{1}H NMR and ESI-TOF mass spectrometry.

^{1}H NMR (400 MHz, D_2O) δ (ppm): 6.33−6.18 (m, 2 H, CH_2=C−), 5.80−5.78. (dd, 1 H, C=CH−), 3.33 (dd, 2 H, α-CH_2), 3.24 (t, 2 H, δ-CH_2), 1.76−1.63 (m, 4 H, β, γ-CH_2).

ESI-TOF [m/z]: 185.14 $(M+H^+)^{1+}$ [calcd. for acryloyl-agmatine 184.13].

*Synthesis of (Agmatinyl)$_6$-maltotriosyl-N-acetyl-amino-hexanoic Acid (Agm$_6$-M-COOH) (**4**).* CuBr (460.47 mg, 3.21 mmol), tris[(2-pyridyl)methyl]amine (TPMA, 932.05 mg, 3.21 mmol), and ascorbic acid (11.3 mg, 0.0642 mmol) were dissolved in 10 mL of anhydrous DMSO and degassed by bubbling nitrogen for 30 min. The solution was then added to 4 mL of a 295.3 mg/mL Acry-Agm solution in degassed DMSO (1181.28 mg, 6.42 mmol), heated to 65 °C, and added to 500 mg of [(isoC$_4$Br)$_6$-M-COOH] (0.321 mmol) previously dissolved in 2 mL of anhydrous DMSO and degassed by nitrogen bubbling. The reaction mixture was stirred for 72 h under nitrogen atmosphere and then exposed to air. After 30 min, the solution was poured into 200 mL of 1:1 v/v diethyl ether/acetone mixture containing 1% v/v of acetic acid to precipitate (agmatinyl)$_6$-maltotriosyl-N-acetyl-amino-hexanoic acid (Agm$_6$-M-COOH). The precipitate was collected and desiccated under vacuum. The precipitate was dissolved in water, dialyzed against water to eliminate unreacted Acry-Agm, and finally freeze-dried. The final product, 542 mg, was analyzed by Sakaguchi assay,[27] ^{1}H NMR (D_2O), FT-IR, and elemental analysis.

The Sakaguchi assay was performed to estimate the guanidinium group content that was derived from a calibration curve obtained with guanidinium solutions in the 0−100 μM range (y = 9.1724x − 0.0075, R^2 = 0.9965).

^{1}H NMR (400 MHz, D_2O) δ (ppm): 3.24 (bm, 12 H, $-CH_2-$), 2.51−2.03 (bm, 12 H, $-CH_2-$), 1.63 (bm, 12H $-CH_2-$), 1.23 [bm 36 H, $-C(CH_3)_2$].

FT-IR: ν (cm^{-1}) 3373 and 3182 [$NHC(NH_2)_2^+$]; 2930 (CH_2); 1750 (C=O); 1300 (C−H bending).

Elemental analysis: found, C 37.58%, H, 5.51%, N, 10.98%; Br, 31.90% (O, 14.03%) [calcd. for (agmatinyl)$_6$-maltotriosyl-N-acetyl-amino-hexanoic acid HBr salt ($C_{98}H_{171}Br_6N_{25}O_{30}$·6HBr): C, 37.43%, H, 5.67%, N, 11.14%, Br, 30.49%, O, 15.26%].

*Synthesis of (Agmatinyl)$_6$-maltotriosyl-N-acetyl-amino-hexanoate-α-methoxy poly(ethylene glycol)$_{5\ kDa}$ (Agm$_6$-M-PEG-OCH$_3$) (**5**).* (Agmatinyl)$_6$-maltotriosyl-N-acetyl-amino-hexanoic acid (Agm$_6$-M-COOH, 500 mg, 0.188 mmol) was dissolved in 10 mL of 1:2 v/v DMSO/100 mM morpholino-ethan-sulfonic acid buffer (MES), pH 4.7. The solution was added of 291.9 mg (1.88 mmol) of 1-ethyl-3-(3-dimethylaminopropyl)carbodiimide (EDC) and 216.3 mg (1.88 mmol) of *N*-hydroxysuccinimide (NHS). The solution was stirred for 30 min and then added to 785 mg of (0.157 mmol) of NH_2−$PEG_{5\ kDa}$-OCH_3 previously dissolved in 1:2 v/v DMSO/100 mM MES buffer, pH 4.7. The solution was stirred for 72 h and then dialyzed against water for 48 h using a 10 kDa MWCO dialysis membrane. The product was lyophilized and characterized by UV−vis spectrophotometric analysis. The final product, 820 mg, was analyzed by Sakaguchi assay and iodine assay for guanidine groups and PEG detection,[28] respectively. The experimental data acquired by the iodine assay were referred to a standard curve obtained with NH_2−$PEG_{5\ kDa}$-OCH_3 (y = 0.0663x − 0.0183, R^2 = 0.9933).

The molar mass of Agm$_6$-M-PEG-OCH_3 was assessed by Malvern Viscotek operated with TSKgel G3000 and TSKgel G4000 paired columns thermostated at 40 °C and eluted with 0.4 M ammonium acetate, pH 4.5, at a flow rate of 0.6 mL/min. The GPC analysis showed the presence of a single peak with an increased molecular weight with respect to the NH_2−$PEG_{5\ kDa}$-OCH_3:

NH_2-PEG_{5kDa}-OCH_3: $M_{n,theor}$ = 5 kDa; $M_{n(GPC)}$ = 4.9 kDa; PDI = 1.08

Agm$_6$-M-PEG-OCH_3: $M_{n,theor}$ = 7.6 kDa; $M_{n(GPC)}$ = 6.8 kDa; PDI = 1.3

Electrophoretic Mobility Shift Assay. Agm$_6$-M-PEG-OCH_3/dsDNA samples were prepared by mixing 2.58 μL of 10 μM scrambled 11 619 Da dsDNA solution (300 ng, 2.58 × 10^{-11} mol) in 10 mM phosphate buffer, 0.15 M NaCl (PBS),

DOI: 10.1021/acs.molpharmaceut.9b00014
Mol. Pharmaceutics 2019, 16, 1678−1693

pH 7.4, with 10 μL of 0.705−7.05 μg/mL Agm_6-M-PEG-OCH_3 solutions in PBS, pH 7.4, to yield 0.5, 1.0, 2.0, 3.0, 4.0, 5.0 N/P ratios. The mixtures were mildly mixed for 30 min at room temperature and then added to 3 μL of loading buffer (50:50 v/v glycerol/water containing 0.25% xylene cyanol). The Agm_6-M-PEG-OCH_3/dsDNA samples were analyzed by gel-electrophoresis using a 12% v/v polyacrylamide gel in 89 mM Tris, 89 mM boric acid, 2 mM EDTA (TBE, 1X) buffer at 100 V. After the completion of the run, the dsDNA was stained by immersion of the gel in a marker solution obtained by diluting 15 μL of GelRed Nucleic Acid Gel Stain 10 000X in 30 mL of Milli-Q water. The gel was then imaged using a PerkinElmer UV-Transilluminator Geliance 600 Imaging System.

Thiazole Orange Association Assay. The degree of Agm_6-M-PEG-OCH_3/dsDNA complexation was evaluated by thiazole orange (TO) exclusion assay following the modified protocol described by Itakura et al.[29] Agm_6-M-PEG-OCH_3/dsDNA mixtures in PBS, pH 7.4, were prepared by adding a fixed volume of Agm_6-M-PEG-OCH_3 solutions at different concentration to a fixed volume of dsDNA solution to yield a final dsDNA concentration of 100 μM and 1.0, 2.0, 3.0, 5.0, 7.0, 10.0 N/P ratios. Then 17.5 μL of Agm_6-M-PEG-OCH_3/dsDNA mixtures were added of 8.25 μL of 100 μM TO solution in DMSO to yield a TO/dsDNA molar ratio of 0.5:1.0. After 15 min, the TO association with dsDNA of the Agm_6-M-PEG-OCH_3/dsDNA polyplex was quantified by fluorescence analysis (λ_{ex} 508 nm, λ_{em} 530 nm).

Isothermal Titration Calorimetry. Isothermal titration calorimetry (ITC) analyses were carried out using a Malvern MicroCal, LLC VP-ITC microcalorimeter (Worcestershire, UK). The ITC analyses were performed under two different titration conditions: (a) 141.2 μM Agm_6-M-PEG-OCH_3 solution was titrated with 40 μM dsDNA solution; (b) 20 μM Agm_6-M-PEG-OCH_3 solution was titrated with 100 μM dsDNA solution. Both Agm_6-M-PEG-OCH_3 and dsDNA solutions were prepared in 10 mM tris(hydroxymethyl)-aminomethane (Tris), 0.15 M NaCl, pH 7.4 and the solutions were degassed and thermostated at 25 °C before the analysis. The ITC analysis was performed at 25 °C. Every 5 min, (a) 10 μL or (b) 6 μL of dsDNA solution was injected into the cell containing 1.5 mL of Agm_6-M-PEG-OCH_3 solutions. Blank analysis was carried out by dsDNA injection into plain buffer and by buffer injection into Agm_6-M-PEG-OCH_3 solutions.

All measurements were replicated three times, and the experimental data obtained by Agm_6-M-PEG-OCH_3 titration with dsDNA were subtracted of the blank profiles and processed with the VP-ITC Microcal Origin 7 software.

Molecular Dynamic Simulations. Atomistic molecular dynamics (MD) simulations were performed to clarify the interaction between dsDNA (19bp) and Agm_6-M-PEG-OCH_3. The following cases were simulated: assemblies with one dsDNA chain and 30 Agm_6-M-PEG-OCH_3 placed in a 150 mM NaCl solution (named "dsDNA-30"); assemblies with 2 dsDNA and 40 Agm_6-M-PEG-OCH_3 placed in a 150 mM NaCl solution (named "2dsDNA-40"). The simulations were performed with NAMD2[30] and mainly described by the CHARMM general force field.[31] The dsDNA were described by a CHARMM36 force field.[32] The particle mesh ewald (PME)[33] method was used for the evaluation of long-range Coulombic interactions. The time step was set to 2.0 fs. The simulations were performed in the NPT ensemble (p = 1 bar and T = 300 K) using the Langevin dynamics (γ_{Lang} = 1 ps^{-1}). After 2000 steps of minimization, ions and water molecules were equilibrated for 2 ns around dsDNA and Agm_6-M-PEG-OCH_3, which were restrained using harmonic forces with a spring constant of 1 kcal/(mol $Å^2$). The last frames of restrained equilibration were used to start simulations of free dsDNA and Agm_6-M-PEG-OCH_3. All the simulations lasted for 20 ns.

Dynamic Light Scattering (DLS) and Zeta Potential Analysis. Dynamic light scattering (DLS) and zeta potential (ζ-potential) analyses were performed at 25 °C using a Malvern Zetasizer NanoZS (Malvern Instruments Ltd., U.K.) supported by a Zetasizer Software (version 6.12). Agm_6-M-PEG-OCH_3 samples (1 mL) in PBS, pH 7.4, at concentrations of 0.01−1 mg/mL were analyzed to assess the copolymer self-association and critical micelle concentration (CMC).[34] Agm_6-M-PEG-OCH_3/dsDNA samples (1 mL) in PBS, pH 7.4, were prepared by mixing 0.5 mL of a 0.5 mg/mL Agm_6-M-PEG-OCH_3 solution with 0.5 mL of a dsDNA solution in the range 1.0−10.0 μM to yield Agm_6-M-PEG-OCH_3/dsDNA mixtures corresponding to 1.0, 2.0, 3.0, 5.0, 7.0, 10.0 N/P ratios.

Transmission Electron Microscopy (TEM). Agm_6-M-PEG-OCH_3/dsDNA polyplexes were prepared by mixing 10 μL of a 5.0 mg/mL Agm_6-M-PEG-OCH_3 solution with 33 or 18.6 μL of a 10 μM dsDNA solution in PBS, pH 7.4, to obtain 3 and 5 N/P ratios, respectively, and the solutions were further diluted to 500 μL with PBS buffer, pH 7.4. The Agm_6-M-PEG-OCH_3/dsDNA samples and Agm_6-M-PEG-OCH_3 were deposited on a small copper grid (400 mesh), covered by "holey film" carbon layer and analyzed in negative staining mode by transmission electron microscopy (TEM, Tecnai G2 microscope, FEI) using 1% w/v uranyl acetate as contrast agent. The aspect ratio (ratio between the major axis and minor axis) of polyplexes was calculated by using ImageJ 1.51g software.

Colloidal Stability of Agm_6-M-PEG-OCH_3/dsDNA Polyplexes. Agm_6-M-PEG-OCH_3/dsDNA samples were prepared by mixing 50 μL of a 5.0 mg/mL Agm_6-M-PEG-OCH_3 solution with 16.4 or 9.85 μL of 100 μM dsDNA to obtain 3 and 5 N/P ratios, respectively, in PBS, pH 7.4, or DMEM supplemented with 10% FBS (fetal bovine serum), 2 mM L-glutamine, 100 IU/mL penicillin, 100 μg/mL streptomycin, and 0.25 μg/mL of amphotericin B (complete DMEM) filtered using MWCO 0.22 μm filter. The samples were maintained at 37 °C and monitored by DLS for 12 h. The experiments were repeated three times, and mean values and standard deviations (SD) were calculated.

Polyanion Displacement Assay. Agm_6-M-PEG-OCH_3/dsDNA 3 and 5 N/P ratio (100 μM dsDNA) polyplexes in PBS buffer, pH 7.4, were incubated for 30 min at room temperature. After incubation, 80 μL of polyplexes was added of 10 mM hyaluronic acid (HA) or dextran sulfate (Dex-SO_4) to yield phosphates/carboxylic acid ratios of the dsDNA/HA mixtures in the range of 1:1−1:100, or phosphates/sulfates ratio of dsDNA/Dex-SO_4 mixtures in the range of 1:0−1:1. All the solutions were prepared in PBS, pH 7.4, and the volumes of all samples were adjusted to 350 μL with the same buffer. After 15 min, 8.25 μL of 100 μM thiazole orange solution in DMSO was added, and fluorescence intensities were measured as described above.

Cell Lines. The human MCF-7 breast adenocarcinoma, human KB cervical carcinoma, murine MC3T3-E1 preosteoblast, and human HeLa cervical carcinoma cell lines were grown at 37 °C, in 5% CO_2 atmosphere, using DMEM

DOI: 10.1021/acs.molpharmaceut.9b00014
Mol. Pharmaceutics 2019, 16, 1678−1693

medium supplemented with 10% FBS (fetal bovine serum), 2 mM L-glutamine, 100 IU/mL penicillin, 100 μg/mL streptomycin, and 0.25 μg/mL amphotericin B.

Cytotoxicity of Agm_6-M-PEG-OCH_3/dsDNA Polyplexes. MCF-7, KB, and MC3T3-E1 cells were seeded in 96-well plates (5×10^3 cell/well). After 24 h, the medium was removed, and the cells were incubated at 37 °C with Agm_6-M-PEG-OCH_3/dsDNA 3 and 5 N/P ratio (125, 250, and 500 nM dsDNA concentration) samples or 125, 250, and 500 nM dsDNA solutions. After 24 and 48 h, the cell survival was assessed by 3-(4,5-dimethylthiazol-2-yl)-2,5-diphenyltetrazolinium bromide (MTT) assay.[35] Twenty microliters of 5 mg/mL MTT solution in PBS was added in each well, and the plates were incubated at 37 °C. After 3 h, the medium was removed, replaced with 200 μL of dimethyl sulfoxide (DMSO), and plates underwent gentle shaking for 15 min at room temperature. The absorbance of each well was read by an ELISA plate reader (Microplate Autoreader EL311, Bio-Tek-Instruments, Winooski, USA) using a test wavelength of 570 nm. All experiments were repeated in triplicate, and the results were derived as mean values with standard deviations (SD).

Flow Cytometry Analysis. The association of the dsDNA and Agm_6-M-PEG-OCH_3/dsDNA polyplexes with MCF-7, KB and MC3T3-E1 cells was investigated by flow cytometric analysis using labeled Cyanine3-dsDNA (Cy3-dsDNA). MCF-7, KB, and MC3T3-E1 cells were seeded in six-well plates at a density of 1.5×10^6 cells/well. After 24 h the medium was removed, and the cells were washed twice with 1 mL of PBS, pH 7.4, and then treated with 500 μL of Agm_6-M-PEG-OCH_3/Cy3-dsDNA 3 5 N/P ratio (125 nM Cy3-dsDNA) polyplex solutions. After 6 h of incubation at 37 °C, the wells were washed three times with 1 mL of PBS, pH 7.4, harvested with trypsin, and transferred into cytometer tubes. After centrifugation at 1500 rpm for 5 min, the supernatants were discharged, and the pellets were redispersed in 300 μL of PBS, pH 7.4, and underwent cytofluorimetric analysis using a BD FACSDiva flow cytometer (Becton, Dickinson and Company, Buccinasco, Milan). Data collection was carried out with 10 000 counts per sample, and the results were processed with BD FACSDiva Software. Results were plotted as arithmetic mean fluorescence intensity.

Confocal Microscopy Observation. MCF-7, KB, and MC3T3-E1 cells were seeded at density of 5×10^4 cells/cm^2 in 24-well plate (Corning, Tewksbury, MA, USA) and grown for 24 h at 37 °C and 5% CO_2. The medium was removed, and the cells were washed with 500 μL of PBS, pH 7.4. Agm_6-M-PEG-OCH_3/Cy3-dsDNA 3 and 5 N/P ratio (500 μL of 125 nM Cy3-dsDNA) polyplexes in complete cell culture medium were prepared by mixing Agm_6-M-PEG-OCH_3 and Cy3-dsDNA solutions as described in the previous section and added to each well. The cells were incubated at 37 °C in the dark for 6 h and then gently washed three times with 500 μL of PBS, pH 7.4. The cells were fixed with 500 μL/well of 1% w/v paraformaldehyde solution in PBS, pH 7.4, for 15 min at room temperature. The wells were washed three times with 500 μL of PBS, pH 7.4, and incubated with 500 μL of a 5.0 μg/mL DAPI solution in PBS for 15 min at room temperature. The DAPI solution was removed, and the fixed cells were washed three times with PBS. To stain the membranes, the fixed cells were treated with 500 μL of a 4.5 μg/mL solution in PBS of wheat germ agglutinin AlexaFluor-488 (WGA-AlexaFluor-488). The wells were washed three times with 300 μL of PBS and three times with 300 μL of Milli-Q water.

The images of samples were acquired using a Zeiss LSM 800 confocal microscope with a 63× oil immersion objective. The samples were irradiated with lasers at 405 nm, 488 nm, and 561 nm to detect DAPI, AlexaFluor-488, and Cy3-dsDNA, respectively.

***In Vitro* Silencing Studies.** *In vitro* siRac1 mediated Rac1 gene expression knockdown by Agm_6-M-PEG-OCH_3/siRac1 polyplexes was evaluated using psiCHECK reporter assay following the psiCHECK-2-based construct preparation for the Rac1 activity as reported by Polyak et al.[36] One copy of a consensus target sequence of Rac1 was cloned into the multiple cloning site located downstream of the *Renilla* luciferase translational stop codon in the 3′-UTR region. HeLa cells (1×10^6) were grown at 37 °C and 5% CO_2. After 24 h, the cells were transfected overnight with 4 μg of Rac1 psiCHECK-2-based plasmids using 4 μL of Lipofectamine 2000. The transfected cells were reseeded in 96-wells plate (150 μL per well) at a final density of 2.5×10^3 cells/well. After 6 h, the cells were treated with the Agm_6-M-PEG-OCH_3/siRac1 polyplexes at 3 and 5 N/P ratio, prepared at increasing concentration of siRac1 (125−500 nM). To evaluate the silencing specificity of the treatment, cells were treated with polyplexes of Agm_6-M-PEG-OCH_3. siRac1 (50 nM) siRac1 complexed with Lipofectamine 2000 was used as positive control. Agm_6-M-PEG-OCH_3 polyplexes of siLuc (scramble siRNA) at increasing siLuc concentrations (125 nM- 500 nM) and siLuc (50 nM) complexed with Lipofectamine 2000 were used as negative control. Untreated cells were used as reference. The cells were incubated with the polyplexes for 72 h. Following the treatment, cells were washed three times with 200 μL of PBS buffer, pH 7.4, and lysed using 50 μL of 1X passive lysis buffer (Promega, Wisconsin, USA). The Rac1 gene silencing was evaluated using Dual-Luciferase Assay kit according to manufacturer procedure and measured by luminescence microplate reader (Mithras LB 940 Multimode Microplate Reader, Berthold Technologies, Germany). The silencing activity results were normalized by the value obtained with the untreated cells transfected with the psiCHECK-2 plasmid only. In parallel, the cell viability of HeLa cells was also performed.

Statistical Analysis. All the results are expressed as mean ± SD. The statistical analysis was performed by using two-way ANOVA. $P < 0.05$ was considered to be significant.

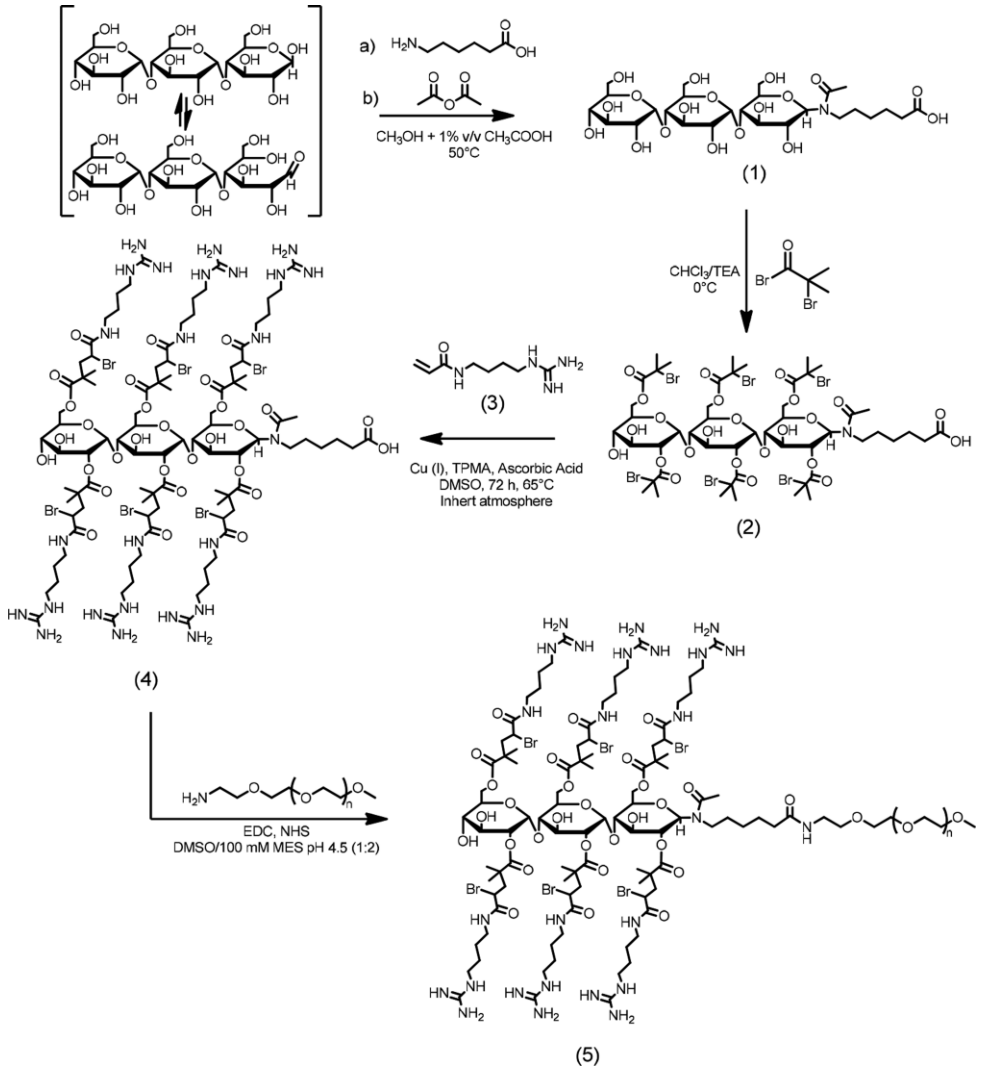
RESULTS AND DISCUSSION

The hybrid "head−tail" bioconjugate reported in this work (Agm_6-M-PEG-OCH_3) was designed to develop an ON vector devoid of intrinsic biological activity and possessing high chemical stability, high biocompatibility, high transfection properties, and tailorable features. Therefore, the star-like shaped cationic "head", which provides for ON association, was designed according to structural evidences reported in the literature: (1) circular disposition of cationic charges in small structures condenses more efficiently with ONs and is more biocompatible than linear polymers;[37] (2) terminal clusters of guanidines in polymeric carriers yield higher cell uptake of polyplexes than guanidines distributed along a polymer backbone;[38] (3) cell penetration peptides used for ON condensation contain about eight guanidyl groups;[39] (4) small cationic polymers are less toxic than high molecular weight cationic macromolecules.[40]

Maltotriose was selected as platform for the construction of the cationic block of the new carrier because it contains 10

DOI: 10.1021/acs.molpharmaceut.9b00014
Mol. Pharmaceutics 2019, 16, 1678−1693

Scheme 1. Synthetic Procedure To Generate Star-like (Agmatinyl)$_6$-maltotriosyl-N-acetyl-amino-hexanoate-PEG$_{5\ kDa}$-OCH$_3$ (Agm$_6$-M-PEG-OCH$_3$)[a]



[a]Agm$_6$-M-COOH and Agm$_6$-M-PEG-OCH$_3$ shown as representative structures.

hydroxyl groups of the C2, C3, C4, and C6 carbons that can be functionalized with guanidyl moieties to generate a star-like oligo-cationic "head". On the other hand, the anomeric carbon in C1 possesses a peculiar reactivity and can be functionalized with a linker for further conjugation with physicochemical or biological modifiers including PEG and targeting agents.

The PEG "tail" was introduced in the carrier structure to enhance the solubility, physical stability, and biocompatibility of micelle-like polyplexes.[41] Furthermore, PEG can provide "stealth" features and prolong the residence time of the polyplexes in the bloodstream, which favor their accumulation into tumors by EPR effect and protect the ONs from enzymatic degradation. Additionally, PEG can be end-tipped with biological modulators or targeting agents to obtain bioselective drug delivery.

Synthesis and Characterization of Agm$_6$-M-PEG-OCH$_3$ Polymer. Agm$_6$-M-PEG-OCH$_3$ was obtained according to the multistep synthesis described in Scheme 1. The intermediates were purified by precipitation or solvent extraction, while the final product was purified by dialysis. Intermediates and final products were characterized by mass spectrometry, FT-IR, NMR, GPC, and colorimetric assays to assess reaction yield, purity, and chemical composition.

In the first step (Scheme 1), the anomeric hydroxyl of maltotriose (M) was derivatized with an amino terminating aliphatic acid (NH$_2$-R-COOH) to generate the intermediate M-COOH (**1**) that can be further functionalized. The resulting Shiff base was stabilized by imine acetylation. The presence of peaks at δ 1.24 and 1.55 ppm in the ^{1}H NMR spectrum indicated the presence of the aliphatic chain on the sugar unit. ^{1}H NMR, ESI-TOF (658.26 Da), and FT-IR (Figure 1a-cSI, Supporting Information) analyses confirmed the chemical identity of the final product (M-COOH), which was obtained with 84.2% molar yield.

In the second step, the hydroxyl groups of M-COOH were derivatized with acryloyl-agmatine (Acry-Agm, **3**) by atom transfer radical polymerization (ATRP) to obtain the oligo-guanidyl polycationic "head".

Acry-Agm was used because agmatine is an endogenous product obtained by decarboxylation of arginine bearing a guanidinium group positively charged under physiological conditions (pK_a ≈ 13).[42] With respect to arginine, agmatine

DOI: 10.1021/acs.molpharmaceut.9b00014
Mol. Pharmaceutics 2019, 16, 1678−1693

does not contain carboxylic groups, which could form intramolecular electrostatic associations with the guanidyl groups and thus shield their charges or decrease the overall positive charge associated with the star-like conjugate required for ON association. Acry-Agm was synthesized by coupling agmatine with acryloyl chloride (Scheme 1SI), and ^{1}H NMR and ESI analyses confirmed the identity of the cationic monomer (Figure3a,bSI).

To derivatize maltotriose with Acry-Agm, the hydroxyl groups of the oligosaccharide were first functionalized with α-bromoisobutyryl bromide, which converted maltotriose into a "star-macroinitiator" [(isoC$_4$Br)$_n$-M-COOH] required for ATRP. The elemental analysis of the resulting product showed that the reaction yielded an average of 6 α-bromoisobutyryl unit out of 10 available −OH groups of M-COOH, which produced the intermediate [(isoC$_4$Br)$_6$-M-COOH] (**2**) (1553 Da mol wt) with 71.7% molar yield. The M-COOH reaction with α-bromoisobutyryl bromide resulted in the reduction of the intensity of the characteristic ^{1}H NMR signals of the sugar (δ 4.70−2.53 ppm, Figure2aSI), and the formation of ester groups was further confirmed by FT-IR (Figure 2bSI), which showed the decrease of the typical −OH signal at 3500 cm^{-1}. The functionalization of the 6 out of 10 hydroxyl groups of maltotriose with α-bromoisobutyryl bromide was in agreement with the results reported in a previous paper[43] and can be ascribed to steric hindrance constrains that prevent the conjugation of 2-bromo-isobutyryl bromide to the vicinal hydroxyl groups of the maltotriose.

The ATRP reaction for Acry-Agm conjugation to [(isoC$_4$Br)$_6$-M-COOH] (Scheme 1SI) was carried out using Cu(I) as catalyst and tris[(2-pyridyl)methyl]amine (TPMA) as ligand in the presence of ascorbic acid under nitrogen flow to prevent Cu(I) oxidation. The reaction resulted in 63.5% molar yield. The ^{1}H NMR spectrum of Agm$_6$-M-COOH (**4**) (Figure 4aSI) was difficult to analyze but displayed characteristic peaks, which demonstrated the formation of a new methylene group between the α-bromoisobutyryl bromide moiety and the derivatized agmatine (δ 2.27 ppm). The presence of the peak at δ 3.24 ppm indicated the presence of agmatine arms on the maltotriosidic scaffold. Notably, in the δ 5−7 ppm region, no peaks were found, indicating the disappearance of acrylic double bond of agmatine and consequently the absence of nonreacted monomer (Figure 5SI). The FT-IR spectrum (Figure 4bSI) of the final product (Agm$_6$-M-COOH) showed the presence of a strong signal at 3373 cm^{-1} corresponding to the guanidinium group. The colorimetric assessment of the guanidinium group by Sakaguchi assay and the elemental analysis demonstrated the presence of a mean of six guanidyl moieties per maltotriose unit (Agm$_6$-M-COOH) indicating that all the activated −OH groups with α-bromoisobutyryl bromide were successfully derivatized with agmatine. It is worth to note that in the literature it is reported that branched structures require lower (n = 6−8) cationic groups than linear structures to yield efficient ON condensation,[24] suggesting that the extent of maltotriose cationization was suitable for ON complexation and delivery.

Finally, Agm$_6$-M-PEG-OCH$_3$ (**5**) was synthesized. The 5 kDa α-methoxy-ω-amino-polyethylene glycol (NH$_2$−PEG$_{5\ kDa}$-OCH$_3$) was conjugated by EDC/NHS to the ε-aminocaproic acid as spacer at the maltotriose anomeric carbon of Agm$_6$-M-COOH cationic head with 65.3% molar yield. The alkylic spacer allowed overcoming the low PEGylation yield obtained by straightforward conjugation of PEG to the anomeric carbon.

The Sakaguchi and iodine assays performed to determine guanidyl groups and PEG, respectively, confirmed that the guanidines/PEG molar ratio in the purified bioconjugate was 6:1. The GPC analysis of Agm$_6$-M-PEG-OCH$_3$ and (Figure 6SI) showed the presence of one species with higher molecular weight (6.8 kDa) and polydispersity index (1.3) with respect to the reference NH$_2$−PEG$_{5\ kDa}$-OCH$_3$ (Mn = 4.8 kDa and 1.08 as PDI). The monomodal narrow distribution of the molecular weights suggested that the bioconjugate possessed homogeneous composition. The underestimated molecular weights detected by GPC of Agm$_6$-M-PEG-OCH$_3$ are ascribable to the different molecular structure of the standard PEG used for the chromatographic column calibration and the oligo-guanidyl bioconjugate. About 35% of the mol wt of Agm$_6$-M-PEG-OCH$_3$ is in fact due to the oligo-guanidyl "head".[44]

Oligonucleotide Complexation. The ability of Agm$_6$-M-PEG-OCH$_3$ to complex oligonucleotides (ONs) was assessed by gel electrophoresis, thiazole orange association assay, and isothermal titration calorimetry (ITC) analysis using 19 bp dsDNA (11 kDa) as model ON. The 19 bp dsDNA was used because of its higher stability compared to siRNAs and its size is similar to the siRNA used in the biological studies reported below.

The gel electrophoresis image of Agm$_6$-M-PEG-OCH$_3$/ON samples with increasing N/P ratio ([guanidyl groups (N) of Agm$_6$-M-PEG-OCH$_3$]/[phosphate groups (P) of ON]) reported in Figure 1A shows that free dsDNA, stained with

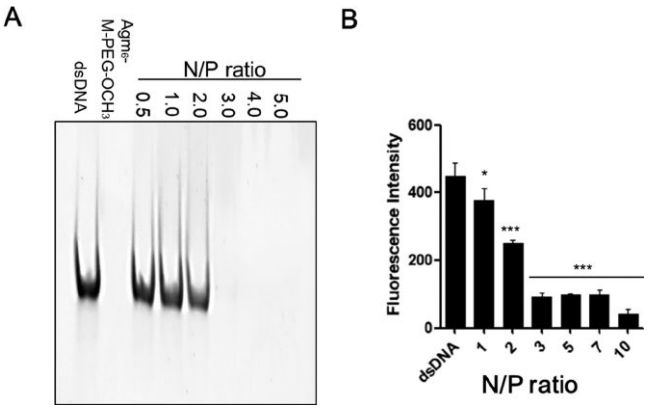


Figure 1. (A) Gel mobility profiles of Agm$_6$-M-PEG-OCH$_3$/dsDNA polyplexes with N/P ratio increasing from 0.5 to 5 at pH 7.4. The samples were run in polyacrylamide gel using TBE as running buffer. (B) Fluorescence intensities of thiazole orange (TO) association with free (noncomplexed) dsDNA polyplexes at increasing N/P ratios in PBS, pH 7.4. The analysis was replicated three times and the data are reported as fluorescence intensity mean ± SD, $*p < 0.05$; $**p < 0.01$; $***p < 0.001$ versus naked dsDNA.

gel red nucleic acid gel stain and visualized using UV-transilluminator as described in our previous work,[45] was not detected at an N/P ratio ≥3 indicating that complete Agm$_6$-M-PEG-OCH$_3$/ON complexation was achieved.

The degree of dsDNA complexation with Agm$_6$-M-PEG-OCH$_3$ was evaluated by thiazole orange (TO) association assay, which is based on the characteristic fluorescence emission at 530 nm resulting from the TO intercalation with free dsDNA in solution. The results displayed in Figure 1B show that the fluorescence of Agm$_6$-M-PEG-OCH$_3$/dsDNA polyplexes significantly decreases as the N/P ratio increases. This is a consequence of the decreased free dsDNA in solution

DOI: 10.1021/acs.molpharmaceut.9b00014
Mol. Pharmaceutics 2019, 16, 1678−1693

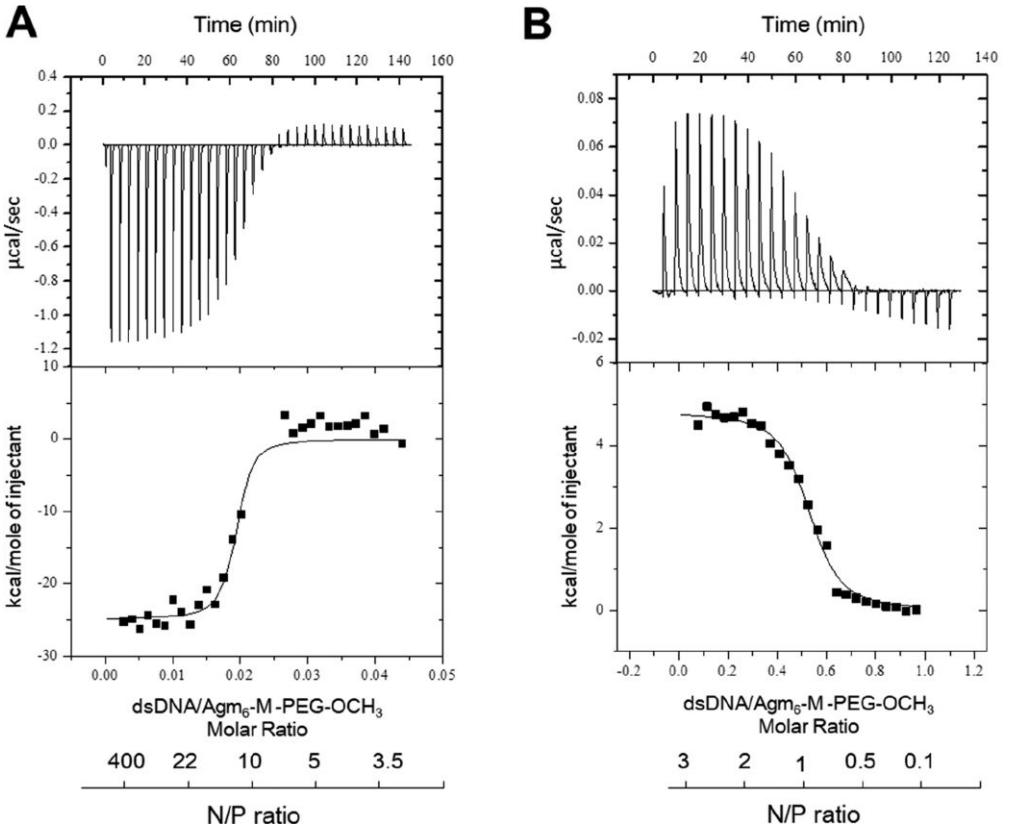


Figure 2. Isothermal titration calorimetry (ITC) profiles of Agm_6-M-PEG-OCH_3/dsDNA association. (A) Agm_6-M-PEG-OCH_3 titration with dsDNA at high N/P ratio. (B) Agm_6-M-PEG-OCH_3 titration with dsDNA at low N/P ratio. The upper panel reports the raw ITC data and the lower panel reports the plot of the heat flow per mole of Agm_6-M-PEG-OCH_3 with dsDNA.

and increased dsDNA complexed with Agm_6-M-PEG-OCH_3. In particular, major fluorescence intensity reduction was observed at a 2−3 N/P ratio indicating that at and above this Agm_6-M-PEG-OCH_3/dsDNA ratio, the ON undergoes extensive association with the macromolecular carrier.

The ON association with the polycationic carrier was further investigated by isothermal calorimetry (ITC) under different titration conditions that highlighted the thermodynamic complexity of the formation of Agm_6-M-PEG-OCH_3/ON polyplexes.

Figure 2A shows that when Agm_6-M-PEG-OCH_3 titration was carried out with dsDNA at high N/P ratios (400−3 N/P ratio range), a typical exothermic ($\Delta H < 0$) behavior was obtained. The experimental data were found to fit one binding site model. The association between the polymer and ON took place under enthalpic control (ΔH $-2.49 \pm 0.07 \times 10^4$ cal/mol), while entropy decreased (ΔS −46.9 cal/mol/deg)[46,47] and the calculated association constant (K_a) was $9.7 \pm 5.45 \times 10^7$ M^{-1}.

Oppositely, the ITC profile obtained in the low N/P ratio range (3−0.1 N/P ratio) reported in Figure 2B shows that under these conditions the dsDNA complexation with Agm_6-M-PEG-OCH_3 is controlled by an entropic process (ΔS 47.4 cal/mol/deg), while the enthalpic content increased (ΔH 4.81 $\pm$ 0.08 $\times$ 10^3 cal/mol)[48,49] and the experimental data were found to fit one binding site model, which yielded an association constant of $6.98 \pm 1.20 \times 10^6$ M^{-1}.

The low N/P ratio for complete association of the dsDNA and the high affinity constant measured by ITC indicate that the carrier possesses high complexation efficiency, which yields a low amount of free carrier (noncomplexed with ON). Note that free carrier is known to be responsible for the toxicity of similar systems.[50]

When Agm_6-M-PEG-OCH_3 was titrated in a high N/P ratio range (N/P 400−3), which provided information about the single ON chain association with multiple Agm_6-M-PEG-OCH_3 molecules, the association process was enthalpy driven ($\Delta H < 0$). However, the ITC profile shows that the Agm_6-M-PEG-OCH_3/dsDNA association undergoes a biphasic process. Initially (above N/P 6), the association is controlled by a characteristic exothermic process with an overall remarkable enthalpy decrease ($\Delta H < 0$) ascribable to electrostatic interactions between the Agm_6-M-PEG-OCH_3 and dsDNA.[51] The heat release observed by dsDNA single injection (siΔH< 0) into the Agm_6-M-PEG-OCH_3 solution decreased as the titration proceeded. The siΔH was nearly 0 at 6 N/P ratio indicating that the enthalpy-driven association was terminated even though ζ-potential and gel electrophoresis analyses showed that, according to the dynamic nature of the association, complete charge balance requires lower N/P ratio. Below 6 N/P ratio, the association proceeds according to a different mechanism. Indeed, the single injection of dsDNA into the cell containing the Agm_6-M-PEG-OCH_3 solution elicited small positive thermal changes (siΔH> 0) indicating that at this point the association process is driven by an entropic mechanism ($\Delta S > 0$) due to the displacement of solvent molecules bound to the polyplexes.[52] In contrast, when the ITC analysis was carried out with low N/P ratio (3−0.1 N/P ratio), the Agm_6-M-PEG-OCH_3 association with a large excess of ON occurred through an endothermic process (ΔH

DOI: 10.1021/acs.molpharmaceut.9b00014
Mol. Pharmaceutics 2019, 16, 1678−1693

> 0) and was driven by a remarkable increase of entropy ($\Delta S > 0$). This result is in agreement with the data obtained in the second phase of titration at high N/P ratio described above (N/P 3−6) and could be due to the combination of conformational changes of ON and Agm_6-M-PEG-OCH_3 and the repulsion among the negative charges of ON at low polymer concentrations.[51] Therefore, when the ON concentration is low with respect to the carrier, the association is driven by an exothermic mechanism. On the contrary, when the ON concentration is high with respect to the carrier, and the carrier is partially associated with the ON to form hindered structures with few charges available for further ON association, the association process is dominated by an entropic mechanism.

Interestingly, the association constant (K_a) calculated at low N/P ratio is about one order of magnitude lower than that calculated at high N/P ratio, which seems to indicate that when a little amount of ON combines with the carrier, only strong interactions are involved in the polyplex formation. On the contrary, when a high amount of ON is combined with the carrier, the binding occurs by both strong and weak associations, which results in an overall lower K_a.

In silico simulations were carried out to get deeper structural insight about the Agm_6-M-PEG-OCH_3/ON interaction.

Figure 3A shows a snapshot of 1 dsDNA molecule and 30 Agm_6-M-PEG-OCH_3 molecules (corresponding to 5 N/P ratio, dsDNA-30) simulated in 150 mM NaCl solution.

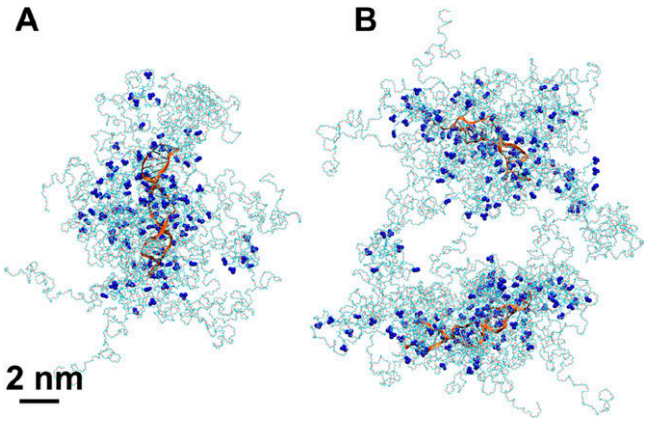


Figure 3. (A) MD simulations of 1 dsDNA and 30 Agm_6-M-PEG-OCH_3 chains. After 20 ns, only 20 Agm_6-M-PEG-OCH_3 assembled around 1 dsDNA, giving a 3 N/P ratio. (B) Two dsDNA strengths wrapped by 40 Agm_6-M-PEG-OCH_3 chains are simulated for 20 ns. The Agm_6-M-PEG-OCH_3 chains become entangled, forming a potential nucleus of a larger molecular complex. dsDNA is shown as orange ribbon with base pair in silver; Agm_6-M-PEG-OCH_3 is shown as a chain with N atoms in blue (highlighted), O atoms in red, C atoms in cyan, S atoms in yellow, Br atoms in pink, and H atoms in white.

After 20 ns of equilibration, the positively charged groups (guanidyl groups) of Agm_6-M-PEG-OCH_3 become oriented toward the negatively charged backbone of dsDNA, while the remaining chains are solvated around the formed polyplex. In total, 20 entangled Agm_6-M-PEG-OCH_3 molecules (out of 30) were found around one dsDNA, which gives a N/P ratio of about 3 (each Agm_6-M-PEG-OCH_3 molecule contains 6 guanidinium groups, while dsDNA has 38 phosphate groups), which is in very good agreement with the complete ON association at 3 N/P molar ratio calculated by gel-electrophoresis, fluorescence analysis, and ITC. The stabilization of a limited number of charged Agm_6-M-PEG-OCH_3 molecules is performed through a terminal self-assembly,[53] where beyond certain total charge of the complex no more charged molecules can join the complex, due to a large Coulombic repulsion. Figure 7SI shows that dsDNA is well covered by these 20 Agm_6-M-PEG-OCH_3 chains.

Next, we took from Figure 3A two polyplexes of 1 dsDNA with 20 Agm_6-M-PEG-OCH_3 (still corresponding to a 3.3 N/P ratio). During 20 ns simulations, some Agm_6-M-PEG-OCH_3 chains bridged the two dsDNA assemblies, forming a larger complex, shown in Figure 3B. We can anticipate that in the same manner like a simple dsDNA complex is stabilized by a terminal self-assembly of Agm_6-M-PEG-OCH_3 chains, a large supercomplex of many dsDNA assemblies is stabilized in a terminal manner.[53] Such a supercomplex can have a rod-shape structure rather than a spherical structure to decrease the Coulombic repulsions between its charged constituents.[54]

Charge, Size, and Shape of Agm_6-M-PEG-OCH_3/dsDNA Polyplexes. The charge (ζ-potential) and size of Agm_6-M-PEG-OCH_3/dsDNA polyplexes were evaluated by dynamic light scattering (DLS) at 25 °C in PBS, pH 7.4, at increasing N/P ratios (from 1 to 10).

The ζ-potential profile reported in Figure 4A shows that the overall positive charge of the polyplexes increased as the N/P ratio increased. At 1 and 2 N/P ratios, the detected ζ-potential of the dsDNA and polymer dispersion was slightly negative, which reflected the dsDNA excess. The polyplex charge switched to positive when the N/P ratio increased from 2 to 3. The ζ-potential profile reflects the composition of the colloidal polyplexes changes with the Agm_6-M-PEG-OCH_3/ON ratio. It is worth noting that a slight positive charge at $N/P > 2$ promotes the polyplexes interaction with the endosomal membrane forming pores or inducing membrane destabilization for the endosomal escape into the cytosol.[55]

Dynamic light scattering (DLS) analyses performed with Agm_6-M-PEG-OCH_3 in the absence of ON did not detect formation of colloidal structures at all copolymer concentrations, and therefore, CMC could not be calculated. On the contrary, the DLS data reported in Figure 4B show that Agm_6-M-PEG-OCH_3 associates with ON to form colloidal structures with sphere volume equivalent similar to other polyplexes obtained with polycationic polymers.[56] The diameter increased from 50 to 75 nm as the N/P ratio increased from 1 to 3, while Figure 4C shows that the polydispersity PDI was similar at all N/P ratio. Note that the diameters calculated by volume-weighted analyses were about 40−80% smaller than that calculated by intensity (Table 1SI). Since the volume weighted/intensity weighted diameter correlation is based on the mathematical correlation of light scattering signal generated under ideal conditions, the observed differences between intensity weighted and volume-weighted diameters can be attributable to the morphological properties of the nanoparticles, suggesting that the nanoparticles do not possess a spherical shape. Above 3 N/P ratio, neither the particle size nor the PDI significantly changed confirming that complete polyplex formation was achieved at 3 N/P ratio.

According to the ITC, gel electrophoresis, DLS, and ζ-potential data, Agm_6-M-PEG-OCH_3/ON polyplexes at 3 and 5 N/P ratios were chosen as the best candidates for ON delivery. These compositions displayed in fact complete ON association to the carrier with high association stability, slight positive charge, and nanometric size.

DOI: 10.1021/acs.molpharmaceut.9b00014
Mol. Pharmaceutics 2019, 16, 1678−1693

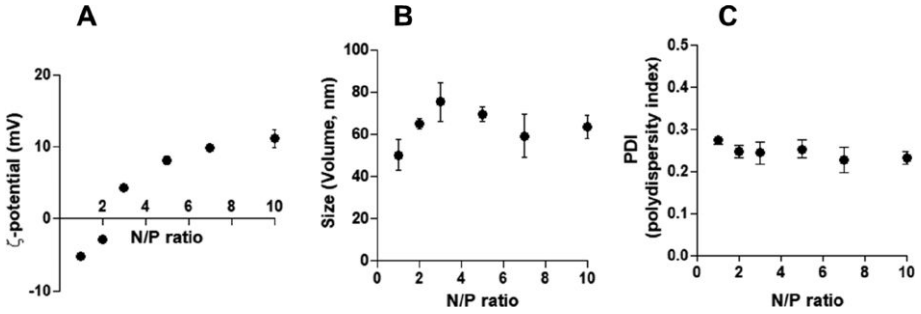


Figure 4. (A) Zeta potential, (B) size, and (C) PDI of Agm_6-M-PEG-OCH_3/dsDNA polyplexes. The analyses were replicated three times, and the data are reported as mean values ± SD.

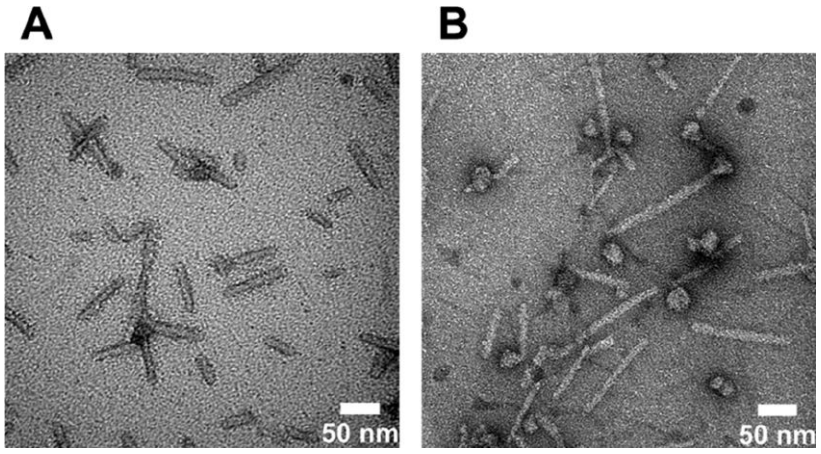


Figure 5. TEM images of Agm_6-M-PEG-OCH_3/ dsDNA polyplexes obtained with (A) 3 N/P ratio and (B) 5 N/P ratio (scale bar: 50 nm).

Transmission electron microscopy (TEM) of Agm_6-M-PEG-OCH_3 in the absence of ONs did not detect the presence of nanostructures. On the contrary, the TEM images of 3 and 5 N/P ratio Agm_6-M-PEG-OCH_3/dsDNA polyplexes reported in Figure 5A and B revealed that the polyplexes have a rod-shape structure, which is in agreement with the DLS results discussed above showing that the polyplexes possess a nonspherical shape and the atomistic molecular dynamics simulations of the experimental systems. The *in silico* studies showed in fact that the decrease of the Coulombic repulsion between the charged constituents of a large supercomplex of many dsDNA assemblies stabilized by terminal self-assembly of Agm_6-M-PEG-OCH_3 chains yields rod-shaped structures rather than spherical structures. As observed for other polycationic carriers used for ON delivery, we speculated that the rod-shaped structures could be originated from the combination of charge distribution of the Agm_6-M-PEG-OCH_3 and the relative stretching of ON molecules into the polyplexes.[57] Importantly, 40−80 nm rod shaped polyplexes have been reported to display longer *in vivo* circulation and more efficient cell up-take and gene silencing[58] than sphere-shaped polyplexes.[59−61]

Interestingly, the Agm_6-M-PEG-OCH_3/ON polyplexes with 3 and 5 N/P ratio showed 3.1 ± 0.9 and 5.7 ± 1.5 aspect ratios (length/width calculated by measuring 100 rods per N/P ratio, Table IISI), respectively, which confirms the ITC results showing that the structure of the complex changes with the Agm_6-M-PEG-OCH_3/dsDNA ratio. In particular, the polyplexes obtained with 3 N/P ratio are thicker and shorter than the polyplexes obtained with 5 N/P ratio indicating that when a high number of ON combines with Agm_6-M-PEG-OCH_3, they conformationally arrange to form a thickset structure. This behavior is in agreement with evidence reported for PEG-*b*-poly(L-lysine) based polyplexes where a higher density of PEG chains on the surface of the complexes, form rods with higher aspect ratio with respect to assemblies at lower PEG density, which may occur for the 5 N/P ratio Agm_6-M-PEG-OCH_3/dsDNA polyplexes.[62,63]

Polyplex Stability. The stability of the Agm_6-M-PEG-OCH_3/dsDNA polyplexes was studied by DLS analyses of polyplexes incubated in PBS and in cell culture medium and by competition assays where the polyplex was incubated with two different polyanionic macromolecules, namely hyaluronic acid (HA) and dextran sulfate (Dex-SO_4). The dsDNA displacement from the polyplexes was assessed by quantification of free dsDNA using thiazole orange (TO) dye.

In PBS, pH 7.4, at 37 °C, 3 and 5 N/P ratio Agm_6-M-PEG-OCH_3/dsDNA polyplexes did not show significant size changes over 12 h. In complete DMEM supplemented with 10% FBS (Figure 8SI), 3 and 5 N/P ratio polyplexes underwent size increase during the first 1.5−2 h of incubation and then remained stable over 12 h. Notably, proteins absorption, which is probably responsible of size increase, does not induce a dissociation of the polyplexes as a result of the forces governing the interactions of the Agm_6-M-PEG-OCH_3 and dsDNA. As reported in several studies, serum proteins could wrap the polyplexes reducing the toxicity and the mononuclear phagocytic system (MPS) recruitment.[64] Therefore, protein association together with the low overall positive charge and the presence of PEG can synergistically bestow polyplexes with high biocompatibility and stealth properties.

DOI: 10.1021/acs.molpharmaceut.9b00014
Mol. Pharmaceutics 2019, 16, 1678−1693

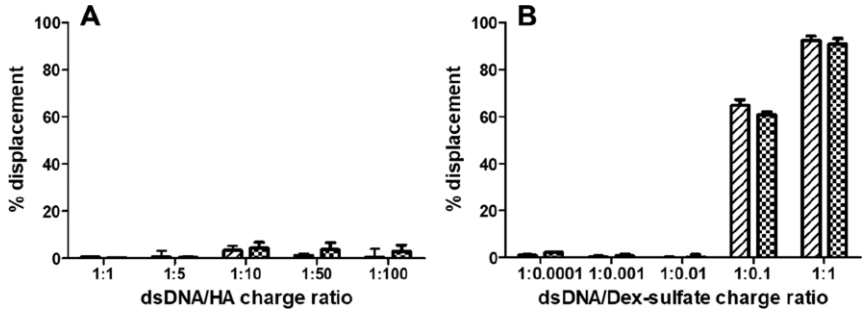


Figure 6. dsDNA displacement profile from Agm_6-M-PEG-OCH_3/dsDNA polyplexes at 3 N/P ratio (diagonal stripes) and 5 N/P ratio (checkers) by (A) hyaluronic acid (HA) and (B) dextran sulfate (Dex-sulfate). The analysis was replicated three times, and the data are reported as mean values ± SD.

The addition of HA to the Agm_6-M-PEG-OCH_3/dsDNA polyplexes did not yield significant fluorescence changes at both N/P ratios tested (Figure 6A) indicating that HA does not affect the polyplex stability. On the contrary, the data reported in Figure 6B show that the incubation of the polyplexes with Dex-SO_4 produced a remarkable increase of fluorescence, demonstrating that the dsDNA was efficiently displaced by the polyanionic macromolecule even at low [dsDNA]/[Dex-SO_4] negative charge ratio. The different displacement obtained with the two polymers is attributable to their different anionic charge. Indeed, Dex-SO_4 has higher number of anionic groups along the polymer chain than hyaluronic acid groups due to the higher number of ionizable groups and the lower pK_a of the former (2 sulfate groups every hexose unit, pK_a < 2) compared to the latter (1 carboxyl group every 2 hexose unit, pK_a ≈ 4−5).[65]

Polyplex Cytotoxicity, Cell Uptake, and Gene Silencing. Cytotoxicity studies were carried out by 24 and 48 h MCF-7, KB, and MC3T3-E1 cell line (breast tumor cells, ovarian tumor cells, and murine preosteoblasts cells, respectively) incubation with increasing concentrations of 3 and 5 N/P ratios Agm_6-M-PEG-OCH_3/dsDNA polyplexes.

The bioconjugate and the two formulations displayed negligible toxicity against the three cell lines after either 24 or 48 h incubation at all the tested polyplex concentrations (Figure 9SI).

The unformulated dsDNA and Agm_6-M-PEG-OCH_3/dsDNA cell association was investigated by flow cytometric and confocal microscopic analyses of KB, MCF-7, and MC3T3-E1 cells incubated for 6 h at 37 °C with dsDNA and 3 and 5 N/P ratios Agm_6-M-PEG-OCH_3/Cy3-dsDNA polyplexes prepared usingCy3 labeled dsDNA (Cy3-dsDNA).

Nonformulated Cy3-dsDNA used as control showed negligible cell association (Figure 10SI). The cytofluorimetric profiles reported in Figure 7 show that both 3 and 5 N/P Agm_6-M-PEG-OCH_3/Cy3-dsDNA polyplexes are efficiently associated with the cells. However, the FACS data indicate that the extent of cell association depends on both polyplexes composition and cell line, similarly to what reported in the literature with other polyplexes.[66,67] The polyplexes targeted KB and MCF-7 cells more efficiently than the MC3T3-E1 cells. Furthermore, in the case of KB and MCF-7 cells, the 3 N/P ratio polyplexes (green profile) associated with the cells more efficiently than the 5 N/P ratio formulation (blue profile). Instead, only very limited cell association was observed with MC3T3-E1 cells either of the 3 or 5 N/P ratio.

The intracellular disposition of Agm_6-M-PEG-OCH_3/dsDNA polyplexes prepared with 3 and 5 N/P ratios after

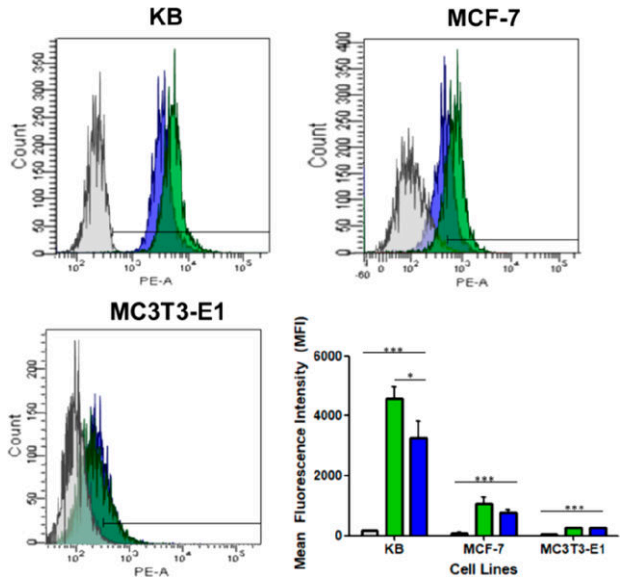


Figure 7. KB, MCF-7, and MC3T3-E1 cell cytofluorimetric profiles after 6 h incubation with Agm_6-M-PEG-OCH_3/Cy3-dsDNA polyplexes obtained with 3 (green profile) and 5 (blue profile) N/P ratios and the corresponding mean fluorescence. Untreated cells were used as control (gray profile). The analysis was replicated three times and the data are reported as fluorescence intensity mean ± SD, $*p < 0.05$; $**p < 0.01$; $***p < 0.001$ versus untreated cells.

incubation with KB, MCF-7, and MC3T3-E1 cells were further investigated by confocal microscopy (Figure 8). The cell membrane was stained with WGA-AlexaFluor488 (green), the nucleus with DAPI (blue), and the Cy3-dsDNA was visualized in red.

The images of KB and MCF-7 cells treated with nonformulated Cy3-dsDNA reported in Figure 8A2 and B2 show only negligible fluorescence of ON (red spots), which seems to be mostly associated with the cell membrane. Figure 8C2 shows no Cy3-dsDNA fluorescence in the case of MC3T3-E1 cells. These results are in agreement with the cytofluorimetric data obtained with Cy3-dsDNA (Figure 10SI). On the contrary, the images of the cells treated with Agm_6-M-PEG-OCH_3/Cy3-dsDNA polyplexes reported in Figure 8A3, A4; B3, B4; and C3, C4 show high localization of Cy3-dsDNA within spots in the cytosol of KB, MCF-7, and MC3T3-E1 mainly restricted to the perinuclear region.[68] The 3 N/P ratio formulation was found to be internalized more efficiently than the 5 N/P ratio formulation, despite the latter is more positively charged than the former (Figure 4A). This result

DOI: 10.1021/acs.molpharmaceut.9b00014
Mol. Pharmaceutics 2019, 16, 1678−1693

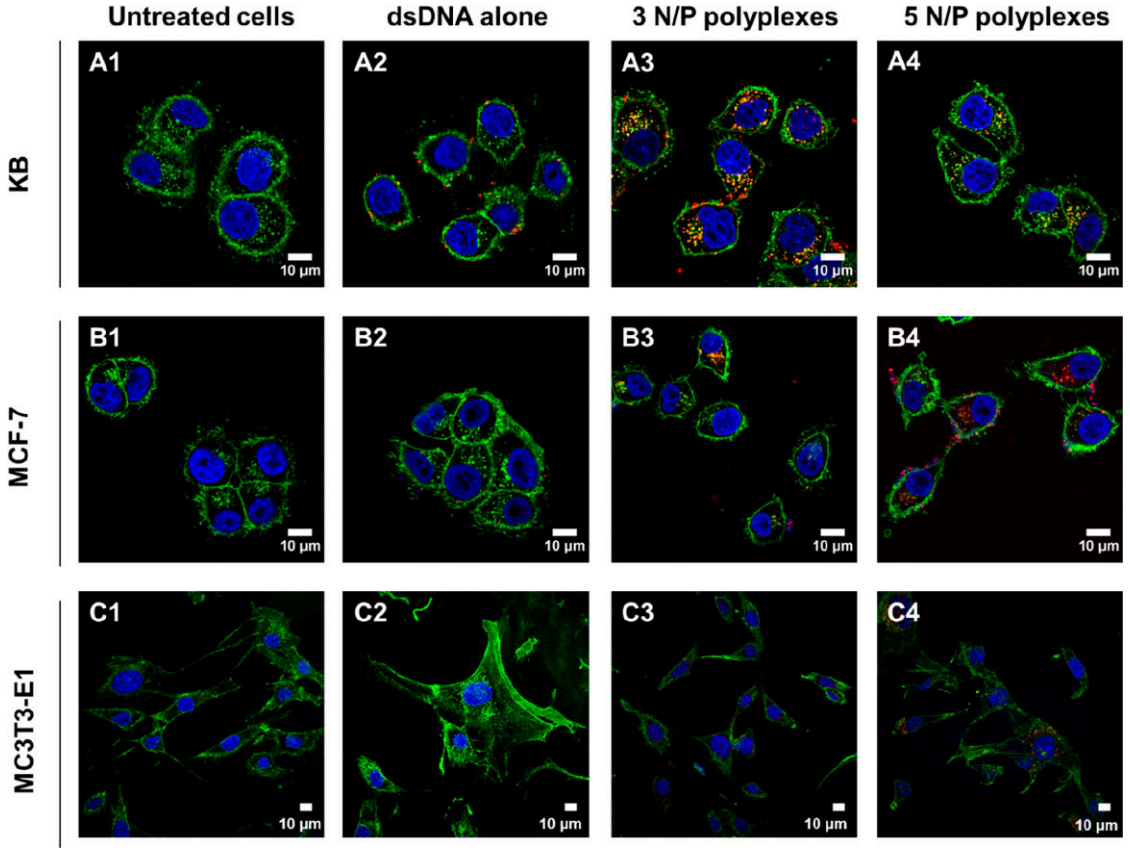


Figure 8. Confocal microscopy images of KB, MCF-7, and MC3T3-E1 cells: (A1, B1, C1) untreated cells (control); (A2, B2, C2) cells treated with Cy3-dsDNA; (A3, B3, C3) cells treated with 3 N/P ratio Agm_6-M-PEG-OCH_3/Cy3-dsDNA polyplexes; (A4, B4, C4) cells treated with 5 N/P ratio Agm_6-M-PEG-OCH_3/Cy3-dsDNA polyplexes. Scale bar indicates 10 μm.

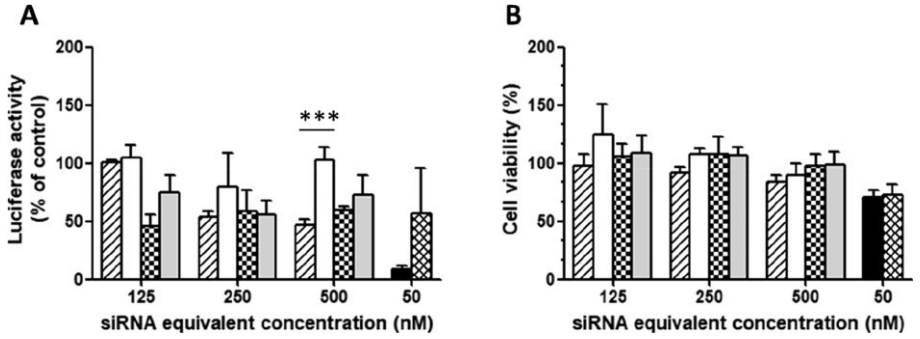


Figure 9. (A) Rac1 gene knockdown and (B) survival of HeLa cells after 72 h of incubation with Agm_6-M-PEG-OCH_3/siRNA polyplexes. HeLa cells were treated with Agm_6-M-PEG-OCH_3/siRac1 polyplexes with 3 N/P ratio (diagonal stripes) and 5 N/P ratio (checkers) at three different concentration (125−500 nM). Agm_6-M-PEG-OCH_3/siLuc polyplexes at 3 N/P ratio (white) and 5 N/P ratio (gray) were used to evaluate the nonspecific silencing. siRac1 (black) and siLuc (crosshatch) at 50 nM either complexed with Lipofectamine 2000 were used as control. Data are reported as mean values ± SD, with $n = 3$ experiments. Statistical analysis $*p < 0.05$; $**p < 0.01$; $***p < 0.001$ versus siLuc complexed polyplexes.

underlines the remarkable influence of the polyplex structure, size, shape, and aspect ratio on the cell uptake. The higher cell uptake was observed with the thick and short Agm_6-M-PEG-OCH_3/ON polyplexes (3 N/P ratio, 3.1 ± 0.9 aspect ratio) with respect to the thin and long structures (5 N/P ratio, 5.7 ± 1.5 aspect ratio), which is in agreement with the evidence reported in the literature that rod-shaped particles preferentially enter the cells through the axial axis perpendicularly oriented to the cell membrane, while the cell penetration with the axial axis parallel to the cell membrane is slower as longer is the particle.[63,66,69−74] The different cell uptake obtained with the three different cell lines suggests that the polyplex internalization undergoes different mechanisms or rates of internalization. Therefore, the elucidation of the mechanisms of cell uptake of these systems is under investigation and will be reported later elsewhere.

Finally, a preliminary evaluation of the Agm_6-M-PEG-OCH_3 ability to deliver intracellularly biologically active ON was performed using Rac1 siRNA as a model ON for gene silencing and HeLa cells, which were selected as model cell line because of their high transfection efficiency due to the phagocytic activity and possibility to select colonies.[75,76] The silencing of Rac1 gene mediated by Agm_6-M-PEG-OCH_3/siRac1 was performed using dual luciferase psiCHECK reporter assay

DOI: 10.1021/acs.molpharmaceut.9b00014
Mol. Pharmaceutics 2019, 16, 1678−1693

and the Dual-Luciferase Assay kit. Rac1 psiCHECK-2 reporter vector is composed of (1) *Renilla* luciferase report gene fused with siRac1 gene sequence, which targets the Rac1 gene, and (2) *Firefly* luciferase, which is the internal control. Decrease in Rac1-gene levels due to siRac1 targeting decreases the *Renilla* luciferase activity, but not the activity of *Firefly* luciferase, which is the internal reference. Therefore, HeLa cells were transfected 24 h before the test with Rac1 psiCHECK-2-based plasmids using Lipofectamine 2000 and *Renilla* and *Firefly* luciferase activities were measured in each of the wells of the 96-wells plate. The transfection was expressed as *Renilla* luciferase activity decrease with respect to *Firefly* luciferase activity, which corresponds to more effective silencing. After 24 h, the transfected HeLa were reseeded and treated for 72 h with 3 and 5 N/P ratio Agm_6-M-PEG-OCH_3/siRac1 polyplexes containing each increasing siRac equivalent doses in the 125−500 nM range. For comparison, siLuc (scramble siRNA devoid of targeting properties and silencing activity for Rac1 gene) was used as negative control to evaluate the off-target silencing. Both siRac and siLuc were also delivered with Lipofectamine 2000, the gold standard for ON delivery which forms spherical assemblies with ONs.[77] Rac1 targeted silencing and siLuc off-target silencing were determined. These results have been confirmed by PCR, which showed that Rac1 mRNA expression was selectively inhibited by cell incubation with Agm_6-M-PEG-OCH_3/siRac1 (Figure 11SI). Cell viability studies were carried out in parallel to verify that Rac1 silencing was not correlated to the cell viability.[36,78]

It is well-known that despite Lipofectamine 2000 is a potent transfection reagent *in vitro*, it is too toxic to be used *in vivo*. The results reported in Figure 9 show that Lipofectamine 2000 used as positive control yielded 92% Rac1 gene knockdown. However, the cell viability results reported in Figure 9B show the high toxicity of Lipofectamine 2000. Furthermore, the results obtained with siLuc (scramble siRNA used as negative control) reported in Figure 9A show that this carrier yields high off-target silencing (50% silencing for the nontargeting siRNA). Toxicity and off-target silencing were abrogated when using our polyplexes. This suggests that our system has the potential to be safer and more selective *in vivo*. The 3 N/P ratio polyplex has a higher selective silencing activity compared to the 5 N/P ratio polyplex, which is in agreement with the higher uptake of the former. The 3 N/P ratio polyplexes showed a dose−response relationship with 53% gene knockdown at 500 nM siRNA equivalent dose, without significant off-target gene knockdown. On the other hand, complexes with 5 N/P ratio show similar Rac1 silencing values but the off-target incidence was higher than the 3 N/P ratio complexes at all the tested concentrations. These results suggest that in the case of 5 N/P ratio complexes, the silencing is mostly not related to the specific siRNA sequence. Importantly, Figure 9B shows that Agm_6-M-PEG-OCH_3/siRNA polyplexes have higher biocompatibility of Lipofectamine 2000 even at 10-times higher concentration.

CONCLUSIONS

The results reported in this paper show that the Agm_6-M-PEG-OCH_3 represents a novel platform with suitable physicochemical, structural, and biopharmaceutical properties for ON delivery. Agm_6-M-PEG-OCH_3 possesses interesting ability to complex oligonucleotides as assessed by different analytical studies. Compared to commercial products, namely Lipofectamine, or other materials described in the literature, Agm_6-M-PEG-OCH_3 displays an excellent biocompatibility and a high potential for *in vivo* application.[79,80] Indeed, the rod-shape structure of the polyplexes generated with the Agm_6-M-PEG-OCH_3 seems to play a key role in the intracellular access of the nanocarrier and thus the delivery of the ON payload. Future studies will involve an "upgrade" strategy to increase the gene knockdown efficiency of this vehicle to better exploit its potential. However, the findings described herein could contribute into the development of a safe and efficient nonviral siRNA delivery system.

ASSOCIATED CONTENT

Supporting Information

The Supporting Information is available free of charge on the ACS Publications website at DOI: 10.1021/acs.molpharmaceut.9b00014.

^{1}H NMR, ESI-TOF mass spectrometry, and FT-IR analysis of compounds 1−5; thickness of Agm_6-M-PEG-OCH_3 chains around dsDNA; stability studies of Agm_6-M-PEG-OCH_3/dsDNA at 3 and 5 N/P ratio; cell viability assay of Agm_6-M-PEG-OCH_3/dsDNA at 3 and 5 N/P ratio on KB, MCF-7, and MC3T3-E1 cells (PDF)

AUTHOR INFORMATION

Corresponding Author

*E-mail: paolo.caliceti@unipd.it.

ORCID

Petr Král: 0000-0003-2992-9027

Stefano Salmaso: 0000-0003-4705-5909

Paolo Caliceti: 0000-0002-2222-9944

Notes

The authors declare no competing financial interest.

ACKNOWLEDGMENTS

This research has been partially supported from EU Horizon 2020 research and Innovation program under the MCS Grant Agreement No. 722717 (OCUTHER). Peter Kral acknowledges the NSF DMR-1506886 grant. The Satchi-Fainaro laboratory's research leading to these results was conducted within the framework of Rimonim Consortium and the MAGNET Program of the Office of the Chief Scientist of the Israel Ministry of Industry, Trade and Labor, and has received partial funding from the European Research Council under the European Union's Seventh Framework Programme (FP/2007-2013)/ERC Consolidator Grant Agreement No. [617445] (PolyDorm).

ABBREVIATIONS

M-COOH, maltotriosyl-N-acetyl-amino-hexanoic acid; $(isoC_4Br)_6$-M-COOH, $(2\text{-bromoisobutyryl})_6$-maltotriosyl-N-acetyl-amino-hexanoic acid; Acry-Agm, acryloyl-agmatine; Agm6-M-COOH, (agmatinyl)6-maltotriosyl-N-acetyl-amino-hexanoic acid; TPMA, tris[(2-pyridyl)methyl]amine; Agm_6-M-PEG-OCH_3, $(agmatinyl)_6$-maltotriosyl-N-acetyl-amino-hexanoate-α-methoxy poly(ethylene glycol)$_5$ kDa; ATRP, atom transfer radical polymerization; MES, morpholino-ethansulfonic acid buffer; EDC, 1-ethyl-3-(3-(dimethylamino)-propyl)carbodiimide; NHS, *N*-hydroxysuccinimide; PBS, phosphate buffered saline; TBE, Tris borate EDTA; DMSO, dimethyl sulfoxide; MWCO, molecular weight cutoff; ON, therapeutic oligonucleotide; N/P ratio, guanidyl groups (N)/

DOI: 10.1021/acs.molpharmaceut.9b00014
Mol. Pharmaceutics 2019, 16, 1678−1693

phosphate groups (P); PEI, polyethilenimine; (pDMAEMA), linear poly [(2-dimethylamino) ethyl methacrylate)]; PEG, poly(ethyleneglycol); EPR, enhanced permeability and retention; GPC, gel permeation chromatography; TO, thiazole orange; ITC, isothermal titration calorimetry; DLS, dynamic light scattering; PDI, polydispersity index; TEM, transmission electron microscopy; MD, atomistic molecular dynamics; PME, particle mesh ewald; HA, hyaluronic acid; Dex-SO4, dextran sulfate; DMEM, Dulbecco's modified Eagle medium; FBS, fetal bovine serum; MTT, 3-(4,5-dimethylthiazol-2-yl)-2,5-diphenyltetrazolium bromide; Cy3-dsDNA, cyanine3-dsDNA; MFI, mean fluorescence intensity

REFERENCES

(1) Cross, D.; Burmester, J. K. Gene therapy for cancer treatment: past, present and future. *Clin. Med. Res.* **2006**, *4* (3), 218−227.

(2) Pack, D. W.; Hoffman, A. S.; Pun, S.; Stayton, P. S. Design and development of polymers for gene delivery. *Nat. Rev. Drug Discovery* **2005**, *4* (7), 581.

(3) Putnam, D. Polymers for gene delivery across length scales. *Nat. Mater.* **2006**, *5* (6), 439.

(4) Geary, R. S.; Norris, D.; Yu, R.; Bennett, C. F. Pharmacokinetics, biodistribution and cell uptake of antisense oligonucleotides. *Adv. Drug Delivery Rev.* **2015**, *87*, 46−51.

(5) Kay, M. A.; Glorioso, J. C.; Naldini, L. Viral vectors for gene therapy: the art of turning infectious agents into vehicles of therapeutics. *Nat. Med.* **2001**, *7* (1), 33.

(6) Baum, C.; Kustikova, O.; Modlich, U.; Li, Z.; Fehse, B. Mutagenesis and oncogenesis by chromosomal insertion of gene transfer vectors. *Hum. Gene Ther.* **2006**, *17* (3), 253−263.

(7) Bessis, N.; GarciaCozar, F.; Boissier, M. Immune responses to gene therapy vectors: influence on vector function and effector mechanisms. *Gene Ther.* **2004**, *11* (S1), S10.

(8) Thomas, C. E.; Ehrhardt, A.; Kay, M. A. Progress and problems with the use of viral vectors for gene therapy. *Nat. Rev. Genet.* **2003**, *4* (5), 346.

(9) Boussif, O.; Lezoualc'h, F.; Zanta, M. A.; Mergny, M. D.; Scherman, D.; Demeneix, B.; Behr, J.-P. A versatile vector for gene and oligonucleotide transfer into cells in culture and in vivo: polyethylenimine. *Proc. Natl. Acad. Sci. U. S. A.* **1995**, *92* (16), 7297−7301.

(10) Whitehead, K. A.; Langer, R.; Anderson, D. G. Knocking down barriers: advances in siRNA delivery. *Nat. Rev. Drug Discovery* **2009**, *8* (2), 129.

(11) Thomas, C. E.; Ehrhardt, A.; Kay, M. A. Progress and problems with the use of viral vectors for gene therapy. *Nat. Rev. Genet.* **2003**, *4* (5), 346.

(12) Luten, J.; Van Nostrum, C. F.; De Smedt, S. C.; Hennink, W. E. Biodegradable polymers as non-viral carriers for plasmid DNA delivery. *J. Controlled Release* **2008**, *126* (2), 97−110.

(13) Matini, T.; Francini, N.; Battocchio, A.; Spain, S. G.; Mantovani, G.; Vicent, M. J.; Sanchis, J.; Gallon, E.; Mastrotto, F.; Salmaso, S.; et al. Synthesis and characterization of variable conformation pH responsive block co-polymers for nucleic acid delivery and targeted cell entry. *Polym. Chem.* **2014**, *5* (5), 1626−1636.

(14) Duncan, R.; Gaspar, R. Nanomedicine (s) under the microscope. *Mol. Pharmaceutics* **2011**, *8* (6), 2101−2141.

(15) Marguet, M.; Bonduelle, C.; Lecommandoux, S. Multicompartmentalized polymeric systems: towards biomimetic cellular structure and function. *Chem. Soc. Rev.* **2013**, *42* (2), 512−529.

(16) Gao, X.-Z.; Huang, L.-B. Cationic liposome-mediated gene transfer. *Gene Ther.* **1995**, *2* (10), 710−722.

(17) Zhang, X.-X.; LaManna, C. M.; Kohman, R. E.; McIntosh, T. J.; Han, X.; Grinstaff, M. W. Lipid-mediated DNA and siRNA transfection efficiency depends on peptide headgroup. *Soft Matter* **2013**, *9* (17), 4472−4479.

(18) Breunig, M.; Lungwitz, U.; Liebl, R.; Fontanari, C.; Klar, J.; Kurtz, A.; Blunk, T.; Goepferich, A. Gene delivery with low molecular weight linear polyethylenimines. *J. Gene Med.* **2005**, *7* (10), 1287−1298.

(19) Mathew, A.; Cao, H.; Collin, E.; Wang, W.; Pandit, A. Hyperbranched PEGmethacrylate linear pDMAEMA block copolymer as an efficient non-viral gene delivery vector. *Int. J. Pharm.* **2012**, *434* (1−2), 99−105.

(20) Nelson, C. E.; Kintzing, J. R.; Hanna, A.; Shannon, J. M.; Gupta, M. K.; Duvall, C. L. Balancing cationic and hydrophobic content of PEGylated siRNA polyplexes enhances endosome escape, stability, blood circulation time, and bioactivity in vivo. *ACS Nano* **2013**, *7* (10), 8870−8880.

(21) Matsumura, Y.; Maeda, H. A new concept for macromolecular therapeutics in cancer chemotherapy: mechanism of tumoritropic accumulation of proteins and the antitumor agent smancs. *Cancer research* **1986**, *46* (12 Part 1), 6387−6392.

(22) Glodde, M.; Sirsi, S. R.; Lutz, G. J. Physiochemical properties of low and high molecular weight poly (ethylene glycol)-grafted poly (ethylene imine) copolymers and their complexes with oligonucleotides. *Biomacromolecules* **2006**, *7* (1), 347−356.

(23) Itaka, K.; Yamauchi, K.; Harada, A.; Nakamura, K.; Kawaguchi, H.; Kataoka, K. Polyion complex micelles from plasmid DNA and poly (ethylene glycol)−poly (l-lysine) block copolymer as serum-tolerable polyplex system: physicochemical properties of micelles relevant to gene transfection efficiency. *Biomaterials* **2003**, *24* (24), 4495−4506.

(24) Ahmed, M. Peptides, polypeptides and peptide−polymer hybrids as nucleic acid carriers. *Biomater. Sci.* **2017**, *5* (11), 2188−2211.

(25) Stenzel-Rosenbaum, M. H.; Davis, T. P.; Chen, V.; Fane, A. G. Synthesis of poly (styrene) star polymers grown from sucrose, glucose, and cyclodextrin cores via living radical polymerization mediated by a half-metallocene iron carbonyl complex. *Macromolecules* **2001**, *34* (16), 5433−5438.

(26) Otiai, M.; Hattori, T.; Kitada, Y.; Kuroda, H.; Oyobikawa, M.; Ichinomiya, S. *Compound, polymer prepared from the compound, and composition comprising the polymer*. U.S. Patent US6703468B1, 2004.

(27) Sakaguchi, S. A new color reaction of protein and arginine. *J. Biochem.* **1925**, *5*, 25−31.

(28) Sims, G. E. C.; Snape, T. J. A method for the estimation of polyethylene glycol in plasma protein fractions. *Anal. Biochem.* **1980**, *107* (1), 60−63.

(29) Itakura, S.; Hama, S.; Matsui, R.; Kogure, K. Effective cytoplasmic release of siRNA from liposomal carriers by controlling the electrostatic interaction of siRNA with a charge-invertible peptide, in response to cytoplasmic pH. *Nanoscale* **2016**, *8* (20), 10649−10658.

(30) Phillips, J. C.; Braun, R.; Wang, W.; Gumbart, J.; Tajkhorshid, E.; Villa, E.; Chipot, C.; Skell, R. D.; Kale, L.; Schulten, K. Scalable molecular dynamics with NAMD. *J. Comput. Chem.* **2005**, *26*, 1781−1802.

(31) Vanommeslaeghe, K.; Hatcher, E.; Acharya, C.; Kundu, S.; Zhong, S.; Shim, J.; Darian, E.; Guvench, O.; Lopes, P.; Vorobyov, I.; Mackerell, A. D. J. CHARMM General Force Field: A Force field for Drug-Like Molecules Compatible with the CHARMM All-Atom Additive Biological Force Field. *J. Comput. Chem.* **2009**, *31*, 671−690.

(32) Hart, K.; Foloppe, N.; Baker, C. M.; Denning, E. J.; Nilsson, L.; MacKerell, A. D., Jr. Optimization of the CHARMM Additive Force Field for DNA: Improved Treatment of the BI/BII Conformational Equilibrium. *J. Chem. Theory Comput.* **2012**, *8* (1), 348−362.

(33) Darden, T.; York, D.; Pedersen, L. Particle mesh Ewald: An N•log(N) method for Ewald sums in large systems. *J. Chem. Phys.* **1993**, *98*, 10089−10092.

(34) Topel, Ö.; Çakır, B. A.; Budama, L.; Hoda, N. Determination of critical micelle concentration of polybutadiene-block-poly (ethyleneoxide) diblock copolymer by fluorescence spectroscopy and dynamic light scattering. *J. Mol. Liq.* **2013**, *177*, 40−43.

DOI: 10.1021/acs.molpharmaceut.9b00014
Mol. Pharmaceutics 2019, 16, 1678−1693

(35) Mosmann, T. Rapid colorimetric assay for cellular growth and survival: application to proliferation and cytotoxicity assays. *J. Immunol. Methods* **1983**, *65* (1−2), 55−63.
(36) Polyak, D.; Krivitsky, A.; Scomparin, A.; Eliyahu, S.; Kalinski, H.; Avkin-Nachum, S.; Satchi-Fainaro, R. Systemic delivery of siRNA by aminated poly (α) glutamate for the treatment of solid tumors. *J. Controlled Release* **2017**, *257*, 132−143.
(37) Wei, H.; Chu, D. S.; Zhao, J.; Pahang, J. A.; Pun, S. H. Synthesis and evaluation of cyclic cationic polymers for nucleic acid delivery. *ACS Macro Lett.* **2013**, *2* (12), 1047−1050.
(38) Favretto, M. E.; Krieg, A.; Schubert, S.; Schubert, U. S.; Brock, R. Multifunctional poly (methacrylate) polyplex libraries: A platform for gene delivery inspired by nature. *J. Controlled Release* **2015**, *209*, 1−11.
(39) Lehto, T.; Ezzat, K.; Wood, M. J.; Andaloussi, S. E. Peptides for nucleic acid delivery. *Adv. Drug Delivery Rev.* **2016**, *106*, 172−182.
(40) Wen, Y.; Pan, S.; Luo, X.; Zhang, X.; Zhang, W.; Feng, M. A biodegradable low molecular weight polyethylenimine derivative as low toxicity and efficient gene vector. *Bioconjugate Chem.* **2009**, *20* (2), 322−332.
(41) Ikeda, Y.; Nagasaki, Y. Impacts of PEGylation on the gene and oligonucleotide delivery system. *J. Appl. Polym. Sci.* **2014**, *131* (9), 1 DOI: 10.1002/app.40293.
(42) Griffiths, M. Z.; Alkorta, I.; Popelier, P. L. Predicting pKa values in aqueous solution for the guanidine functional group from gas phase ab initio bond lengths. *Mol. Inf.* **2013**, *32* (4), 363−376.
(43) Bersani, S.; Salmaso, S.; Mastrotto, F.; Ravazzolo, E.; Semenzato, A.; Caliceti, P. Star-like oligo-arginyl-maltotriosyl derivatives as novel cell-penetrating enhancers for the intracellular delivery of colloidal therapeutic systems. *Bioconjugate Chem.* **2012**, *23* (7), 1415−1425.
(44) Xing, H.; Lu, M.; Xian, L.; Zhang, J.; Yang, T.; Yang, L.; Ding, P. Molecular weight determination of a newly synthesized guanidinylated disulfide-containing poly (amido amine) by gel permeation chromatography. *Asian J. Pharm. Sci.* **2017**, *12* (3), 292−298.
(45) Gallon, E.; Matini, T.; Sasso, L.; Mantovani, G.; Armiñan de Benito, A.; Sanchis, J.; Caliceti, P.; Alexander, C.; Vicent, M. J.; Salmaso, S. Triblock copolymer nanovesicles for pH-responsive targeted delivery and controlled release of siRNA to cancer cells. *Biomacromolecules* **2015**, *16* (7), 1924−1937.
(46) Ma, P. L.; Lavertu, M.; Winnik, F. M.; Buschmann, M. D. New Insights into chitosan− DNA interactions using isothermal titration microcalorimetry. *Biomacromolecules* **2009**, *10* (6), 1490−1499.
(47) Samanta, K.; Jana, P.; Bäcker, S.; Knauer, S.; Schmuck, C. Guanidiniocarbonyl pyrrole (GCP) conjugated PAMAM-G2, a highly efficient vector for gene delivery: the importance of DNA condensation. *Chem. Commun.* **2016**, *52* (84), 12446−12449.
(48) Pozharski, E.; MacDonald, R. C. Thermodynamics of cationic lipid-DNA complex formation as studied by isothermal titration calorimetry. *Biophys. J.* **2002**, *83* (1), 556−565.
(49) Srinivasachari, S.; Liu, Y.; Prevette, L. E.; Reineke, T. M. Effects of trehalose click polymer length on pDNA complex stability and delivery efficacy. *Biomaterials* **2007**, *28* (18), 2885−2898.
(50) Gary, D. J.; Min, J.; Kim, Y.; Park, K.; Won, Y. Y. The effect of N/P ratio on the in vitro and in vivo interaction properties of PEGylated poly [2 (dimethylamino) ethyl methacrylate] based siRNA complexes. *Macromol. Biosci.* **2013**, *13* (8), 1059−1071.
(51) Pozharski, E.; MacDonald, R. C. Lipoplex thermodynamics: determination of DNA-cationic lipoid interaction energies. *Biophys. J.* **2003**, *85* (6), 3969−3978.
(52) Nisha, C.; Manorama, S. V.; Ganguli, M.; Maiti, S.; Kizhakkedathu, J. N. Complexes of poly (ethylene glycol)-based cationic random copolymer and calf thymus DNA: a complete biophysical characterization. *Langmuir* **2004**, *20* (6), 2386−2396.
(53) Yang, M.; Chan, H.; Zhao, G.; Bahng, J. H.; Zhang, P.; Kral, P.; Kotov, N. A. Self-assembly of nanoparticles into biomimetic capsid-like nanoshells. *Nat. Chem.* **2017**, *9* (3), 287−294.
(54) Yeom, J.; Yeom, B.; Chan, H.; Smith, K. W.; Dominguez-Medina, S.; Bahng, J. H.; Zhao, G.; Chang, W. S.; Chang, S. J.; Chuvilin, A.; Melnikau, D.; Rogach, A. L.; Zhang, P.; Link, S.; Kral, P.; Kotov, N. A. Chiral templating of self-assembling nanostructures by circularly polarized light. *Nat. Mater.* **2015**, *14* (1), 66−72.
(55) Varkouhi, A. K.; Scholte, M.; Storm, G.; Haisma, H. J. Endosomal escape pathways for delivery of biologicals. *J. Controlled Release* **2011**, *151* (3), 220−228.
(56) Fernandes, J. C.; Qiu, X.; Winnik, F. M.; Benderdour, M.; Zhang, X.; Dai, K.; Shi, Q. Linear polyethylenimine produced by partial acid hydrolysis of poly (2-ethyl-2-oxazoline) for DNA and siRNA delivery in vitro. *Int. J. Nanomed.* **2013**, *8*, 4091.
(57) Mann, A.; Richa, R.; Ganguli, M. DNA condensation by poly-L-lysine at the single molecule level: role of DNA concentration and polymer length. *J. Controlled Release* **2008**, *125* (3), 252−262.
(58) Xu, D.-M.; Yao, S.-D.; Liu, Y.-B.; Sheng, K.-L.; Hong, J.; Gong, P.-J.; Dong, L. Size-dependent properties of M-PEIs nanogels for gene delivery in cancer cells. *Int. J. Pharm.* **2007**, *338* (1), 291−296.
(59) Zhao, Y.; Wang, Y.; Ran, F.; Cui, Y.; Liu, C.; Zhao, Q.; Gao, Y.; Wang, D.; Wang, S. A comparison between sphere and rod nanoparticles regarding their in vivo biological behavior and pharmacokinetics. *Sci. Rep.* **2017**, *7* (1), 4131.
(60) Gratton, S. E.; Ropp, P. A.; Pohlhaus, P. D.; Luft, J. C.; Madden, V. J.; Napier, M. E.; DeSimone, J. M. The effect of particle design on cellular internalization pathways. *Proc. Natl. Acad. Sci. U. S. A.* **2008**, *105* (33), 11613−11618.
(61) Kolhar, P.; Anselmo, A. C.; Gupta, V.; Pant, K.; Prabhakarpandian, B.; Ruoslahti, E.; Mitragotri, S. Using shape effects to target antibody-coated nanoparticles to lung and brain endothelium. *Proc. Natl. Acad. Sci. U. S. A.* **2013**, *110* (26), 10753−10758.
(62) Williford, J.-M.; Santos, J. L.; Shyam, R.; Mao, H.-Q. Shape control in engineering of polymeric nanoparticles for therapeutic delivery. *Biomater. Sci.* **2015**, *3* (7), 894−907.
(63) Takeda, K. M.; Yamasaki, Y.; Dirisala, A.; Ikeda, S.; Tockary, T. A.; Toh, K.; Osada, K.; Kataoka, K. Effect of shear stress on structure and function of polyplex micelles from poly (ethylene glycol)-poly (l-lysine) block copolymers as systemic gene delivery carrier. *Biomaterials* **2017**, *126*, 31−38.
(64) Mahmoudi, M.; Lynch, I.; Ejtehadi, M. R.; Monopoli, M. P.; Bombelli, F. B.; Laurent, S. Protein nanoparticle interactions: opportunities and challenges. *Chem. Rev.* **2011**, *111* (9), 5610−5637.
(65) Grumezescu, A. M.; Holban, A. M. *Role of Materials Science in Food Bioengineering*; Academic Press, 2018; Vol. *19*.
(66) Liu, X.; Wu, F.; Tian, Y.; Wu, M.; Zhou, Q.; Jiang, S.; Niu, Z. Size dependent cellular uptake of rod-like bionanoparticles with different aspect ratios. *Sci. Rep.* **2016**, *6*, 6.
(67) Agarwal, R.; Singh, V.; Jurney, P.; Shi, L.; Sreenivasan, S.; Roy, K. Mammalian cells preferentially internalize hydrogel nanodiscs over nanorods and use shape-specific uptake mechanisms. *Proc. Natl. Acad. Sci. U. S. A.* **2013**, *110* (43), 17247−17252.
(68) Jiang, X.; Röcker, C.; Hafner, M.; Brandholt, S.; Dörlich, R. M.; Nienhaus, G. U. Endo-and exocytosis of zwitterionic quantum dot nanoparticles by live HeLa cells. *ACS Nano* **2010**, *4* (11), 6787−6797.
(69) He, W.; Xin, X.; Li, Y.; Han, X.; Qin, C.; Yin, L. Rod Shaped Drug Particles for Cancer Therapy: The Importance of Particle Size and Participation of Caveolae Pathway. *Particle & Particle Systems Characterization* **2017**, *34*, 1600371.
(70) Qiu, Y.; Liu, Y.; Wang, L.; Xu, L.; Bai, R.; Ji, Y.; Wu, X.; Zhao, Y.; Li, Y.; Chen, C. Surface chemistry and aspect ratio mediated cellular uptake of Au nanorods. *Biomaterials* **2010**, *31* (30), 7606−7619.
(71) Dasgupta, S.; Auth, T.; Gompper, G. Shape and orientation matter for the cellular uptake of nonspherical particles. *Nano Lett.* **2014**, *14* (2), 687−693.
(72) Chithrani, B. D.; Ghazani, A. A.; Chan, W. C. Determining the size and shape dependence of gold nanoparticle uptake into mammalian cells. *Nano Lett.* **2006**, *6* (4), 662−668.

DOI: 10.1021/acs.molpharmaceut.9b00014
Mol. Pharmaceutics 2019, 16, 1678−1693

(73) Chithrani, B. D.; Chan, W. C. Elucidating the mechanism of cellular uptake and removal of protein-coated gold nanoparticles of different sizes and shapes. *Nano Lett.* **2007**, *7* (6), 1542−1550.
(74) Yameen, B.; Choi, W. I.; Vilos, C.; Swami, A.; Shi, J.; Farokhzad, O. C. Insight into nanoparticle cellular uptake and intracellular targeting. *J. Controlled Release* **2014**, *190*, 485−499.
(75) Kobayashi, M.; Hoshino, T. Phagocytic activity of HeLa cells after thymidine treatment. *Arch. Histol. Cytol.* **1983**, *46* (4), 479−489.
(76) Horibe, T.; Torisawa, A.; Akiyoshi, R.; Hatta-Ohashi, Y.; Suzuki, H.; Kawakami, K. Transfection efficiency of normal and cancer cell lines and monitoring of promoter activity by single cell bioluminescence imaging. *Luminescence* **2014**, *29* (1), 96−100.
(77) Zhang, Y.-M.; Liu, Y.-H.; Zhang, J.; Liu, Q.; Huang, Z.; Yu, X.-Q. Cationic gemini lipids with cyclen headgroups: Interaction with DNA and gene delivery abilities. *RSC Adv.* **2014**, *4* (83), 44261−44268.
(78) Krivitsky, A.; Polyak, D.; Scomparin, A.; Eliyahu, S.; Ofek, P.; Tiram, G.; Kalinski, H.; Avkin-Nachum, S.; Feiner Gracia, N.; Albertazzi, L.; Satchi-Fainaro, R. Amphiphilic poly(alpha)glutamate polymeric micelles for systemic administration of siRNA to tumors. *Nanomedicine* **2018**, *14* (2), 303−315.
(79) Yamano, S.; Dai, J.; Moursi, A. M. Comparison of transfection efficiency of nonviral gene transfer reagents. *Mol. Biotechnol.* **2010**, *46* (3), 287−300.
(80) Breunig, M.; Lungwitz, U.; Liebl, R.; Goepferich, A. Breaking up the correlation between efficacy and toxicity for nonviral gene delivery. *Proc. Natl. Acad. Sci. U. S. A.* **2007**, *104* (36), 14454−14459.

DOI: 10.1021/acs.molpharmaceut.9b00014
Mol. Pharmaceutics 2019, 16, 1678−1693